Demand-driven Beam Densification in Multi-Beam Satellite Communication Systems

Puneeth Jubba Honnaiah*, Eva Lagunas*, Symeon Chatzinotas*, Jens Krause†

*Interdisciplinary Centre for Security, Reliability and Trust (SnT), University of Luxembourg, Luxembourg
email: {puneeth.jubba-honnaiah, eva.lagunas, symeon.chatzinotas}@uni.lu
†SES S.A., Chateau de Betzdorf, Luxemburg
email: jens.krause@ses.com

Abstract—Traditional multi-beam Geostationary (GEO) satellite communication systems provide broadband coverage using a regular grid of fixed spot-beams with uniform 4-colour frequency (4CR) reuse scheme. However, user distribution is non-uniform on ground and, consequently, the demand distribution varies geographically. One potential solution to address high-demand regions is to enhance the satellite beam gain only in those areas. In this paper, we propose the so-called demand driven beam densification approach, which leverages the recent advances in on-board active antenna technologies to generate a higher number of beams over high demand hot-spot areas. Increasing the number of beams result in higher beam overlapping which needs to be carefully considered within the beam frequency planning. In this context, we propose a combination of beam densification, where the number of beams and beam placement is optimized targeting the demand satisfaction objective, followed by frequency-color coding strategy for efficient spectrum and interference management. Supporting results based on numerical simulations show the benefits of the proposed demand driven beam densification in terms of demand matching performance compared with non-densified schemes and regular densification schemes.

Index Terms—Multi-beam High Throughput Satellite Systems, Beam densification, Beam coloring, DVB-S2X.

I. INTRODUCTION

REUSING the spectral resources across sufficiently separated geographical areas has been considered as the baseline design to ensure high spectral efficiency in broadband multi-beam GEO satellite communication systems [1], [2]. Conventional GEO satellite beam-pattern considers a regular spot-beam grid over the targeted coverage area where the so-called 4-color frequency reuse is applied [3], [4]. In other words, satellite communications systems allow using two polarizations concurrently and hence the overall available spectrum is divided into 2 orthogonal blocks and each block is used either with one or the other of orthogonal polarizations, resulting in 4 non-interfering frequency resources.
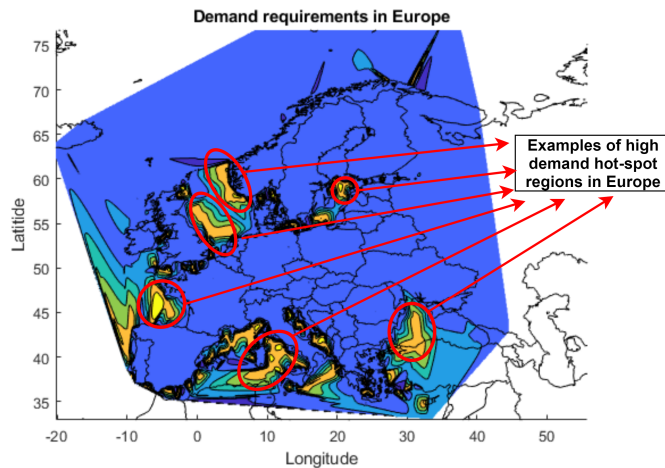
Fig. 1: Demand distribution at 12 PM EST.

Due to rapid population growth and its spatial distribution, the communication traffic is highly non-uniform over the Earth. This has let to hot-spot regions with high capacity requirement over Europe, Eastern and Western United States and South East Asia [5]. For illustration purposes, an example of such high demand hot-spot region generated with the SnT Satellite Traffic Emulator [6] is shown in Figure 1 where high demand hot spots are majorly created by maritime and aeronautical terminals, who represent basically a super user (cluster of large number of users in a flight or ship).

Accordingly, traditional method of regular spot-beam grid with spectral reuse of 4 non-interfering frequency resources fails to provide demand satisfaction at these so called high demand hot-spot regions [7]–[11]. This is because the traditional regular beam grid is designed to provide the same capacity to all beams.

Future high-throughput satellites (HTS) will count with different degrees of freedom to dynamically adapt the supplied capacity to the on-ground demand [12]. Flexibility is typically enabled by two different technologies: (i) frequency flexibility, enabled by on-board channelization of the different beams [13], [14]; and (ii) time flexibility, most commonly known with Beam Hopping (BH), where the same spectral resource is shared by a sub-set of beams that is active for a certain period of time [15], [16]. Power control can also play a role [17], [18], although has minor impact than the frequency/time
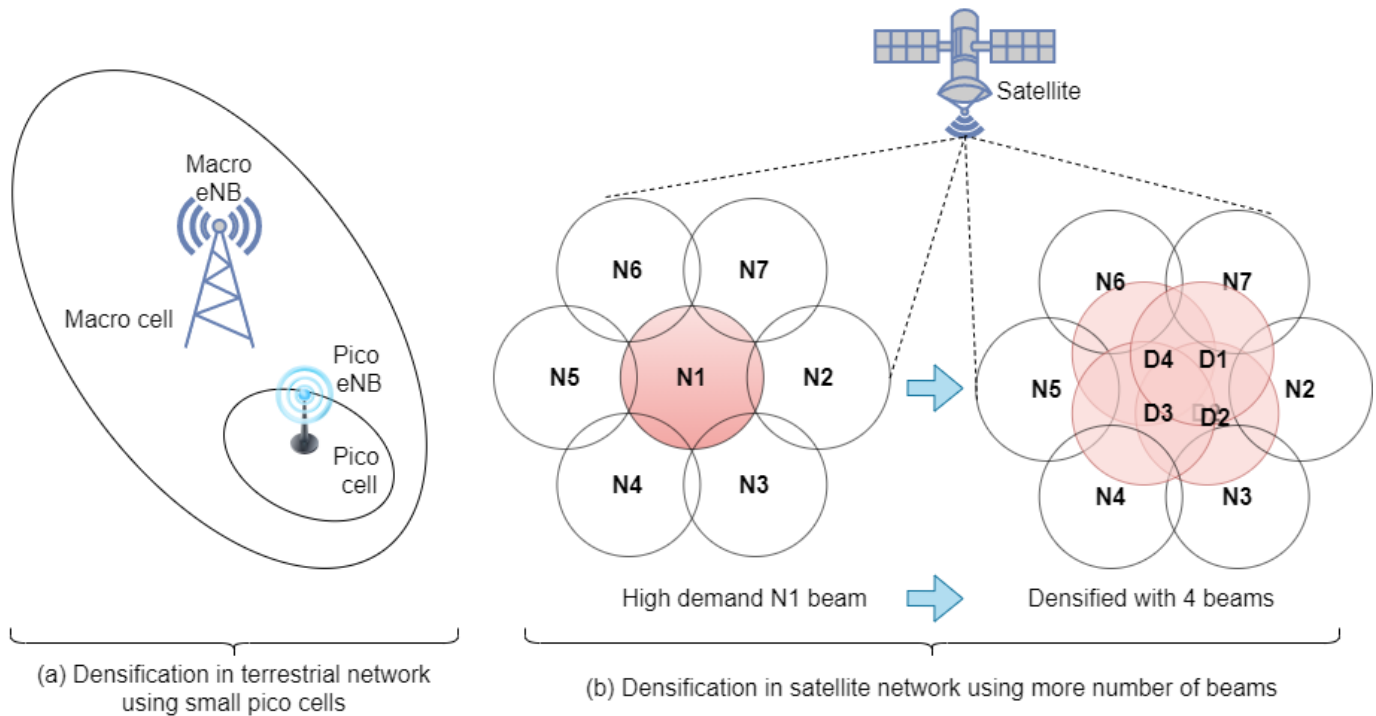
Fig. 2: Beam densification in terrestrial network and satellite network

domain optimization.

Recently, the current state-of-the-art satellite communications see a trend towards the deployment of on-board active antenna systems [19]–[21]. As highlighted in the recent review paper of de Gaudenzi et al. [20], the adoption of active antennas with large number of radiating elements and digital beamforming will open the door to the exploitation of advanced beam pattern design in telecommunication satellites.

A. Motivation

By the end of 2020, 43 million broadband users were connected using communication satellites. Furthermore, this number is expected to be increased to 110 million by the end of 2029. Also, with advancements in very high throughput satellite systems, it is estimated that the satellite connectivity can be provided to more than 697 million broadband users across the globe [22].

Furthermore, the current satellite broadband users are diverse and have unique demand and latency requisites. For example, Fixed Satellite Service (FSS) terminal users including home broadband terminals require web browsing and video streaming traffic. Governmental terminal users require secure communications with ultrareliable traffic. Vehicle to everything (V2X) communication users require low latency ultrareliable traffic. Mobile terrestrial users, broadband aeronautical users and broadband maritime users require continuity in traffic, irrespective of the frequent changes in location/user positions. Accordingly, such mobile users with unevenly distributed users will result in not only non-uniformly distributed

demand profiles but also in time sensitive dynamically changing demand profiles [23]–[26].

Furthermore, satellite operators and service providers agree upon a legal contract named Service-Level Agreement (SLA) that involves volume-based guaranteed broadband rate with availability constraint. Such SLAs will evolve with more sophisticated definitions, including minimum/average achievable throughput, packet loss due to ACM error during configuration changes and failure to meet the latency constraints [27].

Hence, to provide every broadband user with the agreed levels of all the metrics defined in the SLA, especially for nonuniformly distributed demand profiles that are also dynamically changing, is a challenging job for the satellite operators. Hence, there is a need for conventional rigid high throughput multi-beam satellite systems to adapt to the beam profiles. Accordingly, in this work, to make optimum use of the available resources, we aim to deliver capacity where it is required the most. Also, unlike regular capacity maximization approach, we consider demand satisfaction as a key metric.

B. Key enabling technologies for beam densification

1) Trends in On-board Antenna Architectures: The conventional regular beam grid is typically obtained from a Single-Feed Per beam (SFPB) architecture, where each spot beam on the ground is generated by using a single antenna feed element, typically a feed horn. The SFPB architecture is simplistic in terms of hardware but it scales in an unsustainable manner when the number of beams increases [28]. Furthermore, SFPB

requires generally 4 reflectors to generate beams adjacent to each other.

Array antennas are very well established solutions in the general wireless communication domain and it was a question of time that they will break into the satellite architecture. Array antennas can generate customized radiating patterns with high directivity by using a large number of radiating elements. The latter is known as Multi-Feed Per beam (MFPB) architecture [29], because a sub-set of feeds is used to generate one beam. The main advantages of the MFPB architecture is that (i) it requires only 2 reflectors, one for transmission and one for reception; and (ii) combined with a Beam-Forming Network (BFN), it allows to reconfigure the desired beam pattern [30].

Large Array Fed Reflector (AFR), either employing direct center-fed or offset-fed architectures/ focal or defocussed architectures, have been shown promising performance in the satellite communications domain [31]. The offset design is frequently preferred as it has no blockage [32]. Such rapid development of on-board active antenna systems has made it feasible to implement more advanced beam pattern solutions when facing non-uniform geographical demand patters and is the key enabler for beam densification.

2) Digital Beamforming Network (DBN): In the current satellites, conventional analog beamforming networks are used to perform fixed beamforming, where weights are designed in advance and kept constant, resulting in fixed beam patterns and footprints. However, flexibility in coverage is a must for future generation satellite systems and hence, active antenna arrays powered by digital beamforming network (DBN) became a relevant technical solution [33]–[35].

Accordingly, DBN generates reconfigurable beams on Earth, such that the array beam pattern is automatically optimized by adaptively calculating complex weighting coefficients until a certain optimization is achieved. The optimization criteria can be demand satisfaction, maximization of the signal-to-interference-and-noise ratio, minimization of the mean square error (MSE), linear constraint minimum variance (LCMV) and so on. These array beam pattern can also be changed quite significantly from time-slot to time-slot based on the demand profiles [36].

Also, unlike conventional TWTA-based payloads, where per-beam power constraint limits the adaptable designs, DBF enabled advanced payloads provides additional degree of freedom where only the total sum-power constraint has to be respected.

3) Digital Transparent Payload (DTP): In conventional satellite systems, the payloads do not have digital channelization such that the feeder link signal is simply converted in frequency, amplified and forwarded preventing any possibility for flexible channelization and load balancing. However, satellite manufacturers and operators such as SES S.A. are currently deploying advanced Digital Transparent Payload DTP as the de facto platform for future missions [37]. DTP enables digital synthesis of narrow-band user/beam specific carriers from the incoming wideband stream using filter banks and programmable routing of such carriers to end users, offering flexibility in terms of connectivity, channelization and frequency plan [7], [38]–[40].

C. Related works

Beam densification is a new concept in satellite communication. Nevertheless, a similar concept was introduced in terrestrial communications with the advent of the 5th Generation (5G) of cellular networks [41], [42], where the network is densified by placing smaller pico cells in the coverage region of macro cells (Figure 2(a)). Related works include, for example, [43], where the authors discuss industry perspectives of cell densification and the challenges of small cell backhaul, or [44], where the authors explain the benefits of spacial densification in 5G systems.

However, the cell densification of 5G differs in some aspects from the beam densification proposed herein. On one hand, the densification in 5G was imposed by the use of higher frequency bands (from sub-6 GHz to mmWave) [44], which intrinsically provide shorter coverage range. Therefore, the signal loss between the cell center and the cell edge should remain approximately the same as for the non-densified case (in case we keep the same antenna design). On the other hand, shorter wavelengths due to higher frequencies have empowered the design of antenna arrays antennas and unleashed their beamforming capabilities [45], [46]. The latter allows to steer the signal towards specific directions, thus compensating the signal loss with beam pattern gain.

In the case of HTS systems (Figure 2(b)), they have been for a long time operating on the Ka-band for the user link but only recently they are making the technology shift to advanced antenna systems (AAS) [47]. Conventional GEO HTS beam patterns (i.e. without AAS) consider > 100 spot-beams distributed in a regular manner over the coverage area, and with a typical coverage (between beam center and the half-power or -3 dB point of the main lobe) of ~ 300 Km. One of the main disadvantages of such beam planning is the fact that all geographical regions from the coverage region are treated in the same manner. For high demand areas (so-called hot-spots), it may occur that some users are located in the edge of a beam, where they suffer the -3 dB beam pattern loss. Ideally, the beam pattern shall provide similar beam gain over the whole hot-spot area. Hence, the demand driven beam densification emerges as a potential solution to reduce the beam gain difference between user terminal in high demand areas.

The satellite beam densification as described above is relatively new, although some previous works have studied the beam pattern design from different perspective. In particular, the authors of [48], [49] propose an adaptive multi-beam pattern and footprint plan where they design spot beams with flexible size and position based on the spatial clustering of the users in order to increase the demand satisfaction of the users and flexibility of the high throughput satellite system. Furthermore, the authors of [50] use fixed payload and optimize irregular beams coverage and beam pattern to minimize the error between offered and required capacity. Also, the authors of [51] obtain significant gains by increasing or reducing the overlap of signals from adjacent beams at beam edge by adjusting transmission power.

In conventional regular grid of fixed spot beams, 4-colour

frequency reuse coding is used for spectrum management, which divides the total available bandwidth into four sub-frequencies and avoids interference between adjacent beams by not allocating the same sub-frequency to any adjacent beams [7], [8]. However, recent studies in demand driven dynamic beam footprint design [48] and furthermore, beam densification discussed in this paper has given raise to non-regular and overlapping beams. Hence, in such scenarios, the current 4-color coding (spectral reuse of 4 non-interfering frequency resources) will not be able to preclude the inter-beam interference and consequently, affects the capacity performance of the system [9]–[11].

Hence, in irregular and overlapping beams, we must increase color coding factor to reduce the inter-beam interference. However, having high number of colors will result in lower bandwidth availability per beam and reduces the spectral efficiency. On the other hand, having fewer colors will results in higher inter-beam interference. Hence, in this paper, in order to color code with highest spectral efficiency and least inter-beam interference in irregular and overlapped beam footprints, we focus on graph theory based color coding scheme, which on one hand improves the spectral efficiency by choosing least number of colors and on the other, assigns colors to beams for least inter-beam interference.

Furthermore, the beams used for densification herein will retain the shape and size of the non-densified beams with same beam width/antenna gain. This is majorly because, the deployed beams are already as directive as possible (based on the state of the art technologies) and any further attempt to reduce the narrow the beams will increases the complexity of the payload architecture.

D. Contributions

In this work, we focus on frequency and beam pattern flexibility. In particular, we carry out a design trade-off analysis to evaluate the performance of demand driven beam densification which involves increasing the number of beams at high demand hot-spot regions for demand satisfaction. In our design, the power and frequency resources are limited, and the increase in number of beams does not translate into an increase of available resources. While on one hand, beam densification allows to schedule a higher number of users at the same time, it also facilitates the scheduled users to experience better transmit antenna gain. However, the resources per user may diminish with densification, revealing a trade-off design. Furthermore, we study the impact of beam densification on the neighbouring non-densified beams. Also, we focus on employing demand-driven system adaptability by proposing demand driven beam densification and lastly, we propose a novel demand driven frequency reuse strategy using dynamic color coding. The detailed contributions of the paper can be listed as follows:

1) **Regular beam densification**: First of all, we propose and evaluate the potential of a regular beam densification over the target hot-spot area. The latter does not involve any optimization procedure but rather a systematic densification regardless of the particularities of the scenario.

For this, we present a system design trade-off analysis of a specific regular densified beam configuration for different frequency coloring / reuse (including full frequency reuse with and without linear precoding). With this preliminary study, we not only identify the main benefits that can be reached with beam densification but also enumerate the design challenges such as determining the number of beams for the densified area and determining the appropriate frequency reuse scheme. These two points motivate the next contributions listed below, which propose an optimization-based design targeting end-user demand-matching.

2) **Number of beams**: Beam densification involves increasing the number of beams over a certain high demand coverage, while considering the same system power and bandwidth. However, selecting the right number of beams is a challenging task. Choosing too many beams may cause the undesirable effect of increasing the beam overlap (subsequently, the inter-beam interference) and reduction in bandwidth per beam (when higher order frequency reuse is implemented). In this work, we propose a methodology to determine the right number beams for beam densification in accordance to the demand requisites.

3) **Beam Placement**: After the determination of the right number of beams, it is very important to choose the positions of the beams in the high demand coverage region. Traditionally, beams are always chosen equidistant from each other on a grid-like structure (i.e. regular beam grid). In this work, the beam placement is driven by the spatial demand distribution. In particular, we proposed a methodology to find the best beam position by minimizing the error between the demand and offered capacity.

4) **Dynamic frequency reusing scheme**: With the increased number of beams and irregular beam distribution, the frequency plan has to be carefully designed to avoid harmful inter-beam interference. Therefore, the last contribution of our work targets the appropriate beam color coding scheme after densification. Having less "colors" will result in higher bandwidth availability per beam, but may lead to higher inter-beam interference. In this work, we propose a novel graph theory based methodology to both minimize the number of colors and to obtain an optimal frequency plan strategy.

The rest of the paper is organised as follows: In Section II, the system model employing multi-beam high throughput satellite channel is described. In Section III, regular beam densification is explained. Dynamic beam densification to define number of beams and beam positions is explained in Section IV. In Section V, dynamic frequency reuse scheme is discussed. Section VI provides the simulation results, and section VII concludes the paper.

Notation: We use upper-case and lower-case bold-faced letters to denote matrices and vectors, respectively. $\circ$ denotes the element-wise Hadamard operations. $(\cdot)^T$ denotes the transpose of $(\cdot)$. $|\cdot|$ and $\|\cdot\|$ depict the amplitude and Euclidean norm,

respectively.

II. System Model

A. Multi-beam Satellite System

We consider a GEO multi-beam HTS system, where the ground segment is assumed to be a single gateway with ideal feeder link. The purpose of densification is better resource management. This is done in the user link by reducing the resources allocated to low demand cold spot regions and reallocating it to high demand hot spot regions. Hence, densification not necessarily will increase the load on the feeder link. Nevertheless, we do agree that there will be certain degree of impact on the feeder link dimesioning. However, for the sake of focusing on the densification design, we assume ideal feeder link.

In the forward link, the multi-beam satellite system provides service to N single-antenna users using K spot beams where $N >> K$, which are distributed across the coverage area of the satellite. The user distribution on-ground is typically non-uniform, e.g. airport surrounding areas are typically more congested than residential low-populated areas. In addition, the demand requests of users depend on the final service, e.g. satellite backhauling terminals tend to aggregate traffic of many cell phone users resulting in high demand, while residential broadband VSAT terminals typically requests lower traffic.

In this paper, for comparison purposes, we will assume (for some cases) that the satellite system performs precoding on the transmitted signals [52]. In such cases, the precoding is calculated and implemented on ground at the gateway. After that, the precoded signals are transmitted through the feeder link to the satellite and the satellite performs a frequency shift, amplifies and forwards the precoded signals to the final users on ground. Low-complexity linear precoding techniques are considered to alleviate the complexity burden of the gateway [53].

The forward link air interface is assumed to be based on DVB-S2(X) [54], which considers Adaptive Coding and Modulation (ACM) allowing real-time adaptation of transmission parameters according to the link conditions.

B. Multi-beam Satellite Channel

For the methodology presented in this work, it does not matter if the beams are conformed with a single-feed-per-beam (SFPB) architecture or a multiple-feed-per-beam (MFPB)[1]. The users on each beam are served following a Time-Division Multiplex (TDM) scheme, i.e. the entire forward link spectrum is used by one user at a time on each beam. Therefore, in the following, we make use of the same index to indicate served user and beam. The received signal of user n is y_n and is expressed as,

$$y_n = \mathbf{h}_n^T \mathbf{x} + \mathfrak{N}_n, \tag{1}$$

[1]The numerical simulations have been obtained with a SW-emulated Defocused Phased AFR.

where $\mathbf{h}_n \in \mathbb{C}^{K \times 1}$ is the channel vector and includes the channel coefficients seen by user n from all K beams; $\mathbf{x}$ represents the vector of K symbols and $\mathfrak{N}_n$ is the zero-mean thermal noise seen by the user n. By rearranging all the users' received signals in a vector $\mathbf{y} = [y_1 \dots y_K]^T \in \mathbb{C}^{K \times 1}$, and $\mathbf{H} = [\mathbf{h}_1 \dots \mathbf{h}_K]^T \in \mathbb{C}^{K \times K}$, the above model can also be expressed as,

$$\mathbf{y} = \mathbf{H}\mathbf{x} + \boldsymbol{n}, \tag{2}$$

where $\boldsymbol{n} \in \mathbb{C}^{K \times 1}$ is the concatenation of noise samples $\mathfrak{N}_n$.

The channel is defined as $\mathbf{H} = \mathbf{B}e^{\boldsymbol{\Phi}^{\text{LNB}}} e^{\boldsymbol{\Phi}^{(prop)}} \in \mathbb{C}^{K \times K}$, where $\mathbf{B} = [\mathbf{b}_1 \dots \mathbf{b}_N]^T \in \mathbb{R}^{K \times K}$ is the system channel matrix whose $(n,k)^{th}$ component is given by,

$$[\mathbf{b}]_{n,k} = \frac{\sqrt{G_{Rn}G_{kn}}}{(4\pi \frac{\mathfrak{D}_n}{\lambda})}, \tag{3}$$

where λ is the wavelength of the transmission, G_{kn} is the gain of beam k in the direction of user n, G_{Rn} is the user's receive antenna gain and $\mathfrak{D}_n$ is the distance between the satellite and the n-th user.

Our channel has two phase terms introduced by the diagonal matrices $\boldsymbol{\Phi}^{LNB}$ and $\boldsymbol{\Phi}^{(prop)}$. The phase noise introduced by the user's Low-Noise Block (LNB) downconverter, whose diagonal elements ϕ_n^{LNB} are modelled as Gaussian random variable with zero mean and standard deviation of $\sigma_{RX} = 0.24°$ [55]. The diagonal elements of the phase due to RF propagation, ϕ_n^{prop}, depend on the user-to-satellite distance and are modelled as,

$$\phi_n^{prop} = \frac{2\pi}{\lambda}\mathfrak{D}_n \text{ [rad].} \tag{4}$$

The received signal-to interference-plus-noise ratio (SINR) of the n-th user is given by,

$$\gamma_n = \frac{g_{n,n}p_n}{\sum\limits_{k=1,k\neq n}^{K} g_{n,k}p_k + N_o B_n}, \tag{5}$$

where p_n is the power allocated to any user n. B_n is the per-user occupied bandwidth which in the case of unicast systems are equal to per-beam occupied bandwidth B_k. Furthermore, the total system bandwidth is a function of frequency reuse factor. For example, in 4CR frequency reuse generic case, the total system bandwidth is divided into 4 parts : $B_n = B_k = \frac{B_{total}}{4}$. However, considering the benifits of orthogonality introduced by polarization, in this paper, for 4CR frequency reuse, $B_n = B_k = \frac{B_{total}}{2}$. In general, $B_n = B_k = \frac{B_{total}}{\frac{1}{2} \times (number-of-colors)}$. Hence, having higher number of colors will result in lower bandwidth availability per beam. Also, N_o is the noise spectral density and $g_{n,k} = |h_{n,k}|^2$ is the channel power gain.

Furthermore, based on the values of modulation and coding schemes (ACM), DVB-S2X [54] defines a table to map SINR to Spectral Efficiency. Thus, the offered capacity obtained using spectral efficiency (ζ) in DVB-S2X defined table, can be analysed for more practical systems. Hence, in this work, we consider the system capacity based on DVB-S2X and is defined using,

$$C_n = B_n \times \zeta(\gamma_n). \tag{6}$$

As mentioned earlier, sometimes in this work we evaluate full frequency reuse and, as a consequence, we assume that the transmitted symbols are precoded. In that case, $\mathbf{x}$ represents the precoded signal and is given by,

$$\mathbf{x} = \mathbf{Ws}. \tag{7}$$

where $\mathbf{W}$ is the precoding matrix and $\mathbf{s}$ denoted the vector of raw symbols that satisfies $\mathbb{E}[\mathbf{ss}^H] = \mathbf{I}$. The precoding matrix $\mathbf{W}$ is obtained with the well-known Minimum Mean Square Error (MMSE) design (denoted sometimes as regularized zero-forcing) [56], which can be expressed as,

$$\mathbf{W}_{RZF} = \eta \mathbf{H}^{\mathbf{H}} (\mathbf{H}\mathbf{H}^{\mathbf{H}} + \alpha_r \mathbf{I})^{-1}, \tag{8}$$

where α_r is a predefined regularisation factor and η is the power allocation factor that, in our case is defined to comply with the total satellite power constraints,

$$\eta = \sqrt{\frac{P_{tot}}{\text{Trace}(\mathbf{WW}^\dagger)}}, \tag{9}$$

with P_{tot} being the total available power at the satellite.

III. REGULAR BEAM DENSIFICATION

In high demand hot-spot region, beam densification involves increasing the beam pattern gain at edge of the original beam by increasing the number of beams. However, while increasing the number of beams, topological packing and geometrical tractability is a key challenge. Topological packing can be defined as the way the densified beams are placed/packed in the high demand hot-spot region. Furthermore, geometrical tractability is important to keep the operational complexity to minimal.

Inspired by the regular grid beam footprint design of the conventional GEO satellite system, densification can be carried out in a regular fashion. For example, in the Figure 2.B, the high densified N1 beam is replaced by 4 densified beams such that the 4 densified beams (D1, D2, D3 and D4) are placed in a regular fashion around N1 and also equidistant from each other. Such design, on one hand have a high topological packing for its regularity and on the other hand, have good geometrical tractability for its low complexity.

Generally, the beam pattern gain at the beam edge of the non-densified beams (N1 to N7) are at -3dB to -4dB from the beam center. Accordingly, any user scheduled at the beam edge, will suffer from poor beam pattern gain. Furthermore, the densified beams are not narrow beams or directed beams. The densified beams have the same shape and size of the previous non densified beams. However, from the Figure 3.A, after beam densification, the scheduled user will now have better beam pattern gain, in comparison to the non-densified case.

Notwithstanding, from the Figure 3.B, 4 color frequency reuse scheme fails. D3 and N5 (D4 and N4/ D2 and N3) are adjacent beams sharing the same frequency resources and hence cause strong inter-beam interference. Accordingly, in
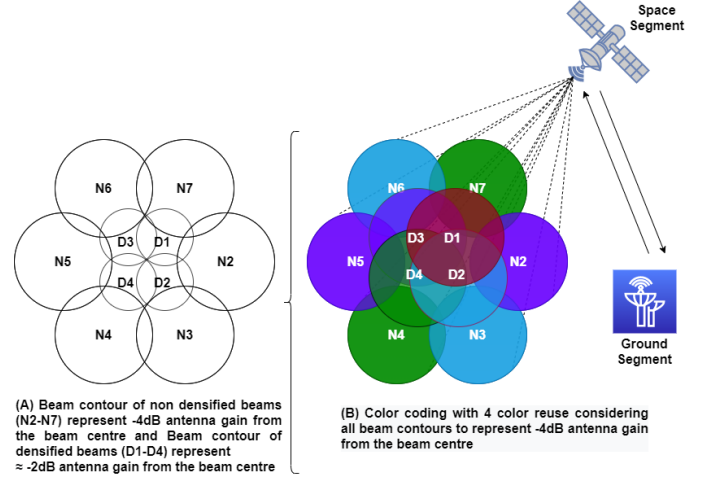

Fig. 3: Regular Beam Densification in the high demand region by replacing one beam with four beams increases inter-beam interference.

this work, we first evaluate the regular beam densification with 4CR frequency reuse and later with 16CR frequency reuse.

The use of 16CR frequency reuse is majorly because, when we regularly densify the beams from 4 to 16, it is natural to think that the color coding will also increase from 4 to 16. The reason is because the interference is kept similar while the user gain is better.

For evaluation purposes, this paper assumes a GEO satellite located at 13 degrees East with a beam pattern obtained with a dedicated software from the European Space Agency (ESA), which has been programmed to model a defocused phased Array-Fed Reflector (AFR). The reflector size is of 2.2m and an array diameter of roughly 1.2m. The antenna array before the reflector is a circular array with 2λ spacing and 511 elements. The pattern has been generated assuming a slight radial amplitude tapering of the array elements. ESA kindly provided the beam pattern to the authors to carry out this study.

As noted in Figure 4, we select 14 beams out of the ESA beam pattern. Beams 3, 6, 7 and 10 are beams with high demand and we call them as parent beams. The shapes and size of the beams in Figure 4 appears to be different for different beams due to the curvature of the Earth and the map projection. Nevertheless, it should be noted that all the beams have same size and shape.

Figure 5, provides the regularly densified beam densification, where the 4 parent beams are replaced by 16 child beams. Furthermore, upon densification of parent beams, the performance of child beams (those beams that replace the parent beams) and the beams around the child beams may be impacted in terms of performance. Therefore, beams around the high-demand area (i.e. the neighbouring beams) will be also considered in our analysis.

IV. DYNAMIC BEAM DENSIFICATION

The homogeneous beam densification, presented as an example in the previous section, can be advantageous when
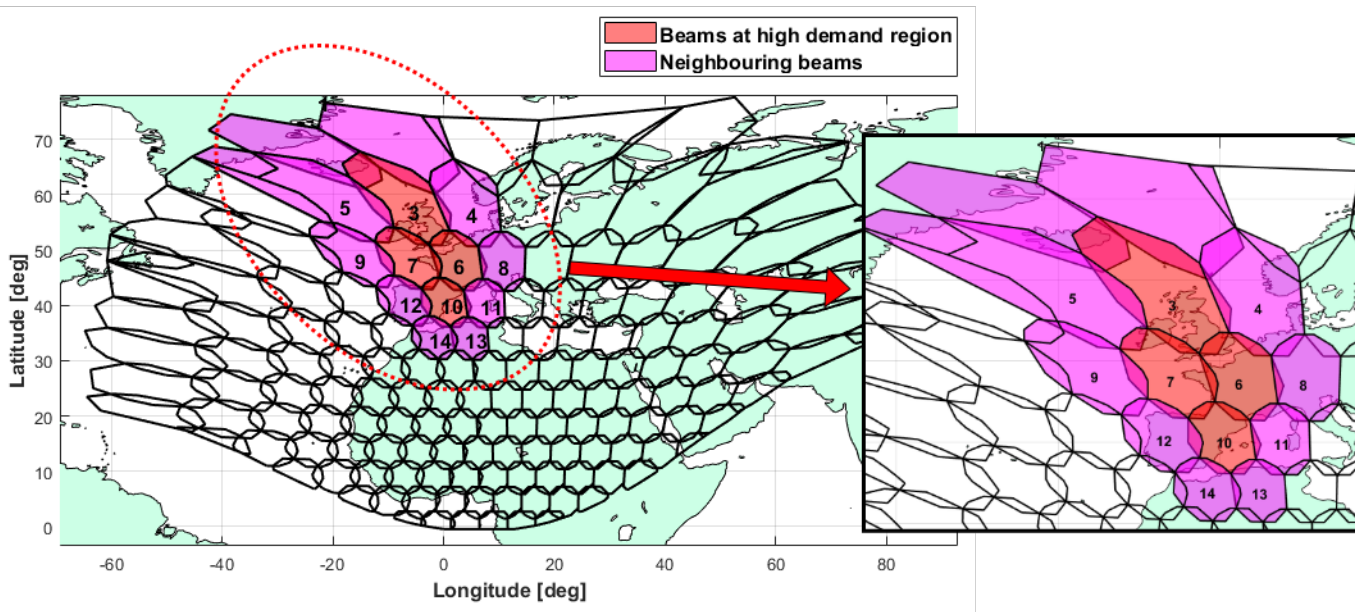
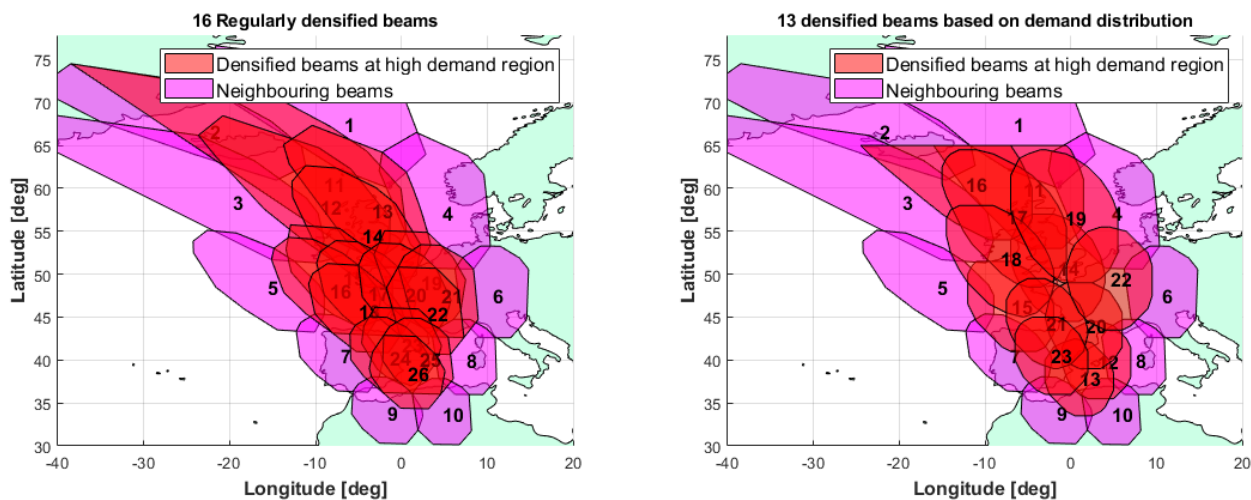Fig. 4: Beams 3, 7, 6 and 10 are the beams in the centre of Europe and with high demand

Fig. 5: Regular beam densification, where 4 beams are re-placed by 16 beams

Fig. 6: Demand driven beam densification where the 4 beams are replaced by 13 beams

the demand of hot-spot regions is itself homogeneously distributed. However, when demand also varies unevenly over the high demand region as shown in Figure 7, it is beneficial to adapt the beam densification scheme for better demand satisfaction.

Also, in the previous densification example, the demand of the hot-spot region was not considered in determining both the number of beams and beam placement. Hence, for dynamic demand requisites, beam densification can be further enhanced by considering demand as a determining factor to decide the number of beams and beam positions.

A. Determining the number of beams

Densifying the high demand hot-spot from 4 beams to 16 beams as shown in Section III, was an arbitrary choice.

Determining the number of beams for densification is not an easy task, as it comes with the following trade-off: With same system power and bandwidth, selecting fewer number of beams may not mitigate enough the beam pattern gain loss between users in beam center and users in beam edge but may reduce the beam overlap between adjacent beams; on the other hand, selecting too many beams may be beneficial in terms of offering good beam pattern gain to all users but may result in higher inter-beam interference. Hence there is a need for effective algorithm to define the number of beams as a function of demand. Accordingly, we define the the number of beams as K and formulate an optimization problem as below,
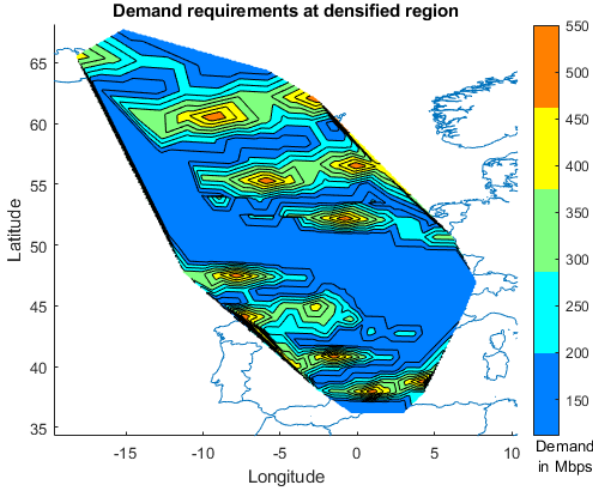
Fig. 7: Uneven demand distribution at the densified region

$$\min_{K} \sum_{k=1}^{K} (D_k - C_k)^2; \tag{10a}$$

$$s.t. \quad C_k = B_k \times \zeta(\gamma_k) \tag{10b}$$

$$K_{min} \leq K \leq K_{max} \tag{10c}$$

where the objective function is to reduce the error between the overall beam demand $D_k = \sum_{n \in \mathcal{G}^k} d_n$, $\mathcal{G}^k$ denoting the set of users belonging to beam k, and beam offered capacity C_k. In unicast systems, $C_k = C_n$, $B_k = B_n$ and $\zeta(\gamma_k) = \zeta(\gamma_n)$ and is defined in Equation (6).

However, by its virtue, the objective function chooses highest number of beams that best satisfy the beam demand. Furthermore, the constraint having interference signal in the denominator limits the choice of the number of beams to a realistic value. Nevertheless, the problem (10a) is NP hard problem because of the interference signal in the denominator of the constraint (as it is a function of the number of beams). Hence, we make use of cluster analysis [57], [58].

In cluster analysis, increasing the number of clusters will reduce the error in user clustering. Accordingly, when we consider each cluster element as a cluster, we can obtain zero clustering error which is not an ideal or practical approach as such huge number of beams will have strong inter-beam interference. Hence the decision of K is a balance between the highest compression of the cluster elements using a single cluster, and the highest efficiency by assigning each user to its own cluster.

Authors of [59]–[61] have focused on finding the ideal number of clusters for a given data set. In particular, Variance Ratio Criterion (VRC) or Calinski-Harabasz(CH) index is used, i.e. the ratio of the sum of between-clusters dispersion and of inter-cluster dispersion for all clusters. The higher the CH index, the better the clustering.

However, the CH index does not assign weights to its cluster point and hence, will not be an ideal scheme for demand satisfaction. Accordingly, to adapt the CH index to our particular problem (10a), we define spatially distributed demand

grid of J points with d_j indicating the demand of the jth grid point. Then we define beam demand as $D_k = \sum_{j=1}^{J} d_j$. Furthermore, we define the overall system demand defined as, $D_{sys} = \sum_{k=1}^{K} D_k$.

Later, we update the regular CH index to account for the users' demand in the form of Weighted Calinski-Harabasz (WCH) index, defined by,

$$WCH(K) = \frac{\sum_{k=1}^{K} n_k \|\mathfrak{M}_k - \mathfrak{M}\|^2}{\sum_{k=1}^{K} \sum_{j \in \mathcal{G}_j} \|\Theta_j - \mathfrak{M}_k\|^2 \times \frac{D_k}{D_{sys}}} \frac{(J - K)}{(K - 1)} \tag{11}$$

where n_k is the number of spatially distributed demand grid points in a cluster k, $\mathfrak{M}_k$ is the centroid of the cluster k, $\mathfrak{M}$ is the geographical mean of the spatially distributed demand grid points, $\|\mathfrak{M}_k - \mathfrak{M}\|$ is the Euclidean distance between the two vectors and Θ_j is the position of the spatially distributed demand grid point j.

The proposed procedure is a good suboptimal solution to determine the number of beam based on Equation (11) and is given in Procedure 1, where high demand hot-spot region is divided into different values of K clusters using weighted k-means clustering [48] and then WCH index for the K cluster is computed. Any value for K that maximizes CH index is considered as good number of cluster.

The complexity of the procedure 1 as $\mathcal{O}(K_e wnkd)$ where K_e is the number of k values tested, for w iterations, k centers, and n points in d dimensions.

Procedure 1: Evaluate cluster size using WCH criteria

Input	: X, K_{min}, K_{max}
Output	: K

for $K= K_{min}$ **to** K_{max} **do**
    1. Obtain K clusters using weighted k-means algorithm [48].
    2. Evaluate WCH index for the K clusters using,
$$WCH(K) = \frac{\sum_{k=1}^{K} n_k \|\mathfrak{M}_k - \mathfrak{M}\|^2}{\sum_{k=1}^{K} \sum_{j \in \mathcal{G}_j} \|\Theta_j - \mathfrak{M}_k\|^2 \times \frac{D_k}{D_{sys}}} \frac{(J - K)}{(K - 1)}$$
end
3. Evaluate ideal value of K using $K = \max(CH(k))$

Apparently, from [48], it is evident that better demand satisfaction is obtained when the total demand is more evenly distributed among all the beams. Hence, we modify the popular Calinski and Harabasz test by replacing the step 1 of the test i.e. classical k-means clustering to weighted-k means clustering mentioned in [48]. This test on one hand evaluates for high "between-clusters variance" and low "inter-cluster variance" along with evenly distributing demand across all the beams. Hence, the proposed technique is a good suboptimal solution in finding the "number of beams."

As illustrative example, we have executed Procedure 1 with $K_{min} = 4$ and $K_{max} = 16$ and considering the high-demand area indicated in Figure 7, which was originally covered in Figure 4 by beams 3, 6, 7 and 10. The results are shown in Figure 8, where it can be observed that $K = 13$ maximizes the WCH value and hence is considered as good sub-optimal number of beams for this particular example.
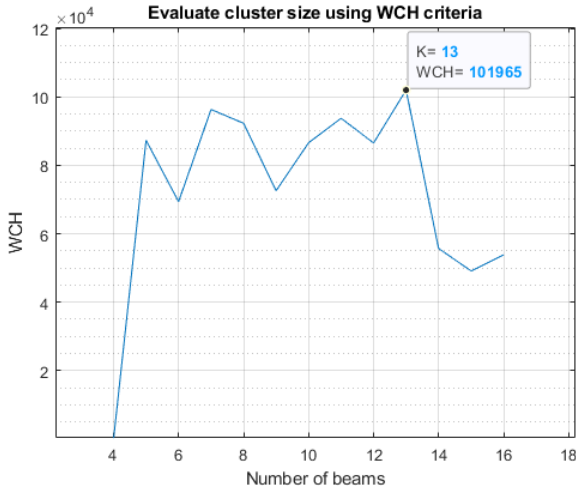
Fig. 8: Finding the number of beams

B. Determining beam placement

After determining the number of beams for densification, the next crucial step is to determine the beam center position. In regular densification, the densified child beams were positioned regularly equidistant from each other. However, in this section, by considering the demand requisites, we propose a novel beam positioning scheme that provides the most demand satisfaction.

Once the number of beams is identified, the reader may note that a possible beam placement solution can be obtained simply by executing step 1 of Procedure 1.

In this section, we provide a generalization of Step 1, by considering a grid of possible beam center locations different than the grid points considered by the weighted K-means proposed in [28]. In particular, assuming that the user-to-beam assignment is extracted from Procedure 1, we can address the beam center positioning problem independently for each beam[2].

Furthermore, the user distribution on the surface of the earth is nonuniform. Accordingly, in section IV-A, we had defined spatially distributed demand grid of J points with d_j indicating the demand of the jth grid point. Nevertheless, to find the demand-based beam position, we define another grid called beam grid of I points with θ_i being the beam center. Obviously, the easier choice is to have both demand grid and beam grid of same dimension. However, the granularity of beam grid depends on antenna constraints and the granularity of the demand grid is governed by the demand requisites. Hence, we define them separately using i and j.

Our intension was to obtain maximum demand satisfaction $\forall j$ in every beam k. Hence in coherence with [48], we find θ_i as below,

$$\min_{\theta_i} \sum_{j=1}^{J} d_j - c_{j,\theta_i} \tag{12}$$

[2]Note that the interference issues will be addressed in the frequency planning section

and further place the beam k at position of θ_i.

Accordingly, Figure 6 provides the demand driven beam densification where the 4 beams are replaced by 13 beams for the demand profile shown in Figure 7.

V. DYNAMIC FREQUENCY REUSING SCHEME

In conventional regular grid of fixed spot beams, 4-colour frequency reuse coding is used for spectrum management, which divides the total available bandwidth into four sub-frequencies and avoids interference between adjacent beams by not allocating the same sub-frequency to any adjacent beams. However, recent studies in demand driven dynamic beam footprint design and furthermore, beam densification discussed in this paper has given raise to non-regular and overlapping beams. Hence, in such scenarios, the current 4-color coding (spectral reuse of 4 non-interfering frequency resources) will not be able to preclude the inter-beam interference and consequently, affects the capacity performance of the system [7]–[11].

Hence, in irregular and overlapping beams, we must increase color coding factor to reduce the inter-beam interference. However, having high number of colors will result in lower bandwidth availability per beam and reduces the spectral efficiency. On the other hand, having fewer colors will results in higher inter-beam interference. Hence, in this paper, in order to color code with highest spectral efficiency and least inter-beam interference in irregular and overlapped beam footprints, we focus on graph theory based color coding scheme, which on one hand improves the spectral efficiency by choosing least number of colors and on the other, assigns colors to beams for least inter-beam interference.

A. Graph construction

Upon densification, to reduce inter-beam interference, we can use color code of higher order. For example, in Figure 3.B, upon densification, one beam is densified by four beams, 4CR frequency reuse will not be efficient to reduce the inter-beam interference and accordingly, beams can be coded with 7 colors such that no two adjacent beams have the same color.

However, increasing the number of colours will decrease the offered channel bandwidth and consequently affects the offered capacity. Hence, it is important to color code with minimum number of colors. In this case of Figure 3.B, we could compute the colors manually because the number of colors and the beams are few. However, as shown in Figure 9, when multiple adjacent beams are densified, color coding is not a straightforward approach. Hence, we propose the use of graph theory to compute the optimal number of colours and colouring strategy.

The 14 beams of Figure 9 can be represented using graph theory by the graph $G = (V, e)$, where nodes V represents the beams and edges e connect to interfering beams. The graph G is as shown in left part of Figure 10. However, upon densification, the number of nodes increase from 14 to 26, where 4 beams are replaced by 16 beams where the traffic demand is high. The densified graph G is as shown in right part of Figure 10.
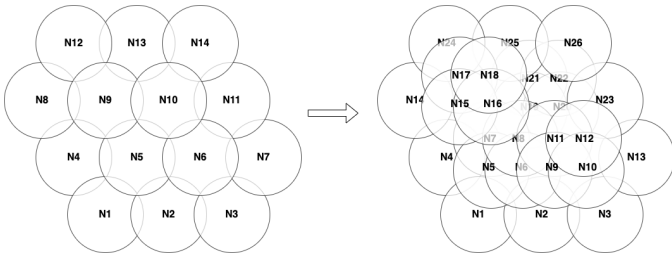
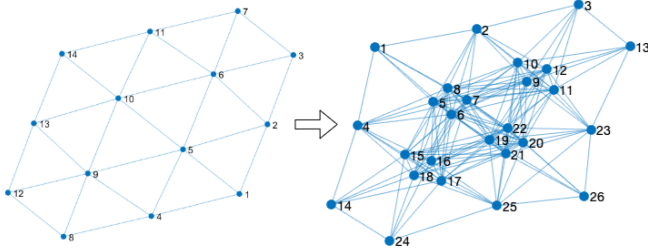Fig. 9: Non densified 14 beams to the left and densified 26 beams to the right

Fig. 10: Graph representing non densified 14 beams on the left and graph representing densified 26 beams on the right

However, to construct such graphs, it is important to define beam adjacency. Accordingly in this work, we define beam adjacency using Euclidean distance. We consider a satellite system with K number of beams and formulate a logical adjacency matrix, $\mathbf{A}$ which is of dimension $K \times K$. The entries of $\mathbf{A}$ define the adjacency between all K beams of the system. Accordingly each element $a_{(i,j)}$ of the $K \times K$ matrix is set to binary 1 if beam i is adjacent to beam j, and binary 0 otherwise. Furthermore, we use Euclidean distance to define adjacency between the beams such that each element $a_{(i,j)}$ is defined as,

$$a_{(i,j)} = \begin{cases} 1, & \text{if } d(i,j) <= d_{\min} \\ 0, & \text{otherwise} \end{cases} \quad (13)$$

where $d(i,j)$ is the distance between any two beams i and j. Hence, if the distance between two beams is less or equal to $d_{\min}$, the beams are said to be adjacent to each other. The minimum distance $d_{\min}$ is chosen wisely with reference to traditional spot beam beam footprint with a hexagonal grid layout.

We define $G = \{V, E\}$ as undirected graph that represents the satellite network, where, $V = \{v_1, v_2..., v_k\}$, is set of all nodes in G. Any edge $e(k, k')$ between two nodes v_k and $v_{k'}$ exist, when beams k and k' are adjacent to each other and can cause potential inter-beam interference.

The set of all such edges in G is denoted as E. $G = \{V, E\}$ can easily be constructed using logical adjacency matrix, $\mathbf{A}$. The entries $a_{(i,j)}$ in $\mathbf{A}$ specify the network of connections (edges) between the nodes of the graph. The location of each nonzero entry in $\mathbf{A}$ specifies an edge between two nodes.

For example, logical adjacency matrix, $\mathbf{A}$ for the beams

mentioned in Figure 2.B is as below,

$$\begin{array}{ccccccc} N1 & N2 & N3 & N4 & N5 & N6 & N7 \end{array}$$
$$\begin{pmatrix} 0 & 1 & 1 & 1 & 1 & 1 & 1 \\ 1 & 0 & 1 & 0 & 0 & 0 & 1 \\ 1 & 1 & 0 & 1 & 0 & 0 & 0 \\ 1 & 0 & 1 & 0 & 1 & 0 & 0 \\ 1 & 0 & 0 & 1 & 0 & 1 & 0 \\ 1 & 0 & 0 & 0 & 1 & 0 & 1 \\ 1 & 1 & 0 & 0 & 0 & 1 & 0 \end{pmatrix} \begin{array}{c} N1 \\ N2 \\ N3 \\ N4 \\ N5 \\ N6 \\ N7 \end{array}$$

and the graph that represents the logical adjacency matrix, $\mathbf{A}$ is shown in Figure 11 where the nodes represent the beams and the edges represent the adjacency between the beams.
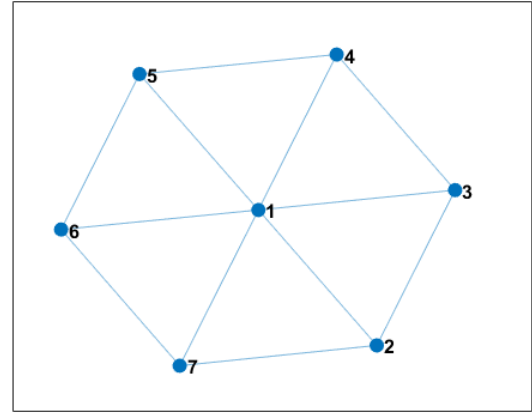

Fig. 11: Graph obtained from the adjacency matrix to the beams in Figure 1.

B. Optimized color coding

In order to avoid inter-beam interference, we need to color the nodes of the graph G, such that no two adjacent nodes have the same color. Also, to reuse frequencies, we need to find the minimum chromatic number $\chi(G)$, which is smallest number of colors needed to color G. Accordingly, we formulate an optimization problem as,

$$\min_{\{V_1, V_2...V_{\chi(G)}\}} \chi(G); \quad (14a)$$

$$s.t. \quad V_c = \{v_k : e(k, k') = 0 \quad \forall k, k'\} \quad (14b)$$

$$V_{c1} \cap V_{c2} = \emptyset \quad \forall c1 \neq c2 \quad (14c)$$

$$\bigcup_{c=1}^{\chi(G)} V_c = V \quad (14d)$$

$$1 \leq \chi(G) \leq \chi(G)_{max} \quad (14e)$$

where the objective function is to minimize the chromatic number (number of colors) and V_C is the set of all nodes of same color. The first constraint ensures that no two adjacent nodes of graph G will have same color. The second constraint is to ensure that no vertex is assigned with two different colors.

The third constraint is to ensure the union of subsets is the full set of vertices and hence all the vertices are coloured. The last constraint sets an upper bound for the number of colors required.

In order to solve the problem 14a, we define binary variables $x_{v_i c}$ such that when a vertex v_i is assigned a color c, $x_{v_i c}$ takes the value 1; otherwise, $x_{v_i c}$ takes the value 0. Besides, binary variable y_c=1 indicates that color c has been used, i.e., set V_c contains at least one vertex; otherwise, V_c is empty and V_c, indicating that color k was not required. We hence can reformulate the 14a as,

$$\min \sum_{c=1}^{\chi(G)_{max}} y_c \qquad (15a)$$

$$s.t. \quad y_c \in \{0,1\}; \quad c = 1, ..., \chi(G)_{max} \qquad (15b)$$

$$\sum_{c=1}^{\chi(G)_{max}} x_{v_i c} = 1; \quad \forall v_i \in V \qquad (15c)$$

$$x_{v_i c} \in \{0,1\} \quad \forall v_i \in V \qquad (15d)$$

$$x_{v_i c} + x_{v_j c} \le y_c \quad \forall \{v_i, v_j\} \in E \qquad (15e)$$

The first and the third constraint in this formulation indicates that y_c and $x_{v_i c}$ are binary variables. The second constraint ensures that exactly one color is assigned to each vertex. The last constraint connects variables x and y, allowing coloring with color c only if $y_c = 1$, and forbids the endpoints of any edge $\{i, j\}$, vertices i and j, from having the same color simultaneously.

The problem was solved by branch-and-bound method using PySCIPOpt 4.2.0 [62], a Python interface for Solving Constraint Integer Programs (SCIP) [63].

VI. SIMULATION PARAMETERS AND RESULTS

The considered antenna pattern (kindly provided by the European Space Agency, ESA) corresponds to a GEO 13°E satellite operating at the Ka exclusive band 19.7 to 20.2 GHz. A summary of simulation parameters are shown in Table I. For simulation, we consider unicast scheduling with K users scheduled in K beams where each of the user position is randomly selected. Accordingly, before densification, we schedule 4 users in the high demand region using 4 beams. After densification with regularly densified beams, we use 16 beams to schedule 16 users in the same high demand region. Similarly, when we densify with demand based densification, we use 13 beams to schedule 13 users in the same high demand region. Also, for reliable result evaluation, we perform Monte Carlo simulations for 100 iterations and consider mean values for our result analysis.

The result analysis is organised as follows: Firstly, we assess the beam patterns in VI.A, then evaluate the impact of densification with 4 color frequency reuse in section VI.B, then in VI.C we study the impact of densification with full frequency reuse and precoding. Later, we study the impact of densification with dynamic frequency reuse in VI.D and Finally, in VI.E we analyse the impact of densification on neighbouring beam.
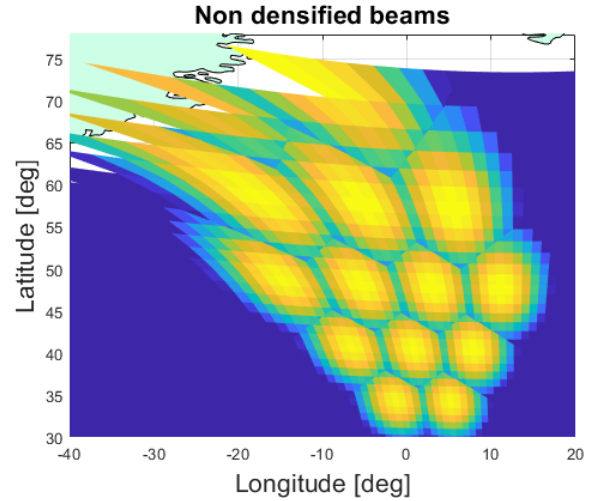

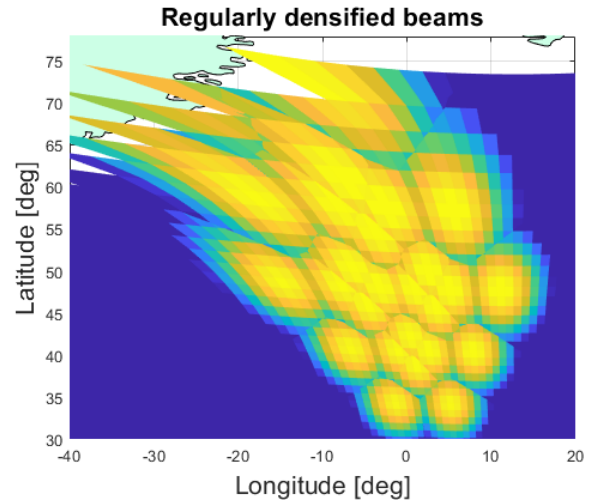Fig. 12: Antenna Gain of non densified beams

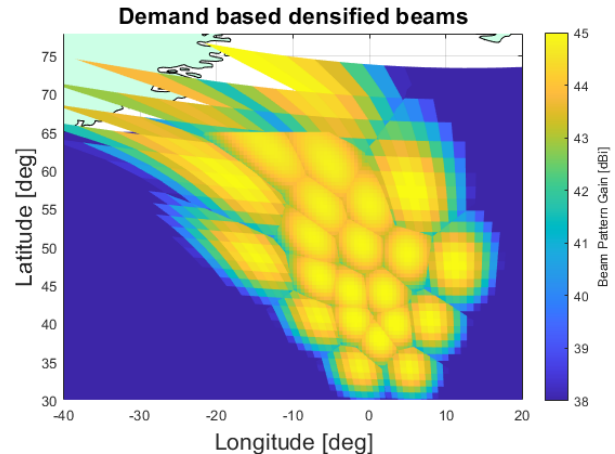Fig. 13: Improved antenna gain by regularly densified 16 beams

Fig. 14: Improved antenna gain by demand driven densified 13 beams

TABLE I: Simulation Parameters

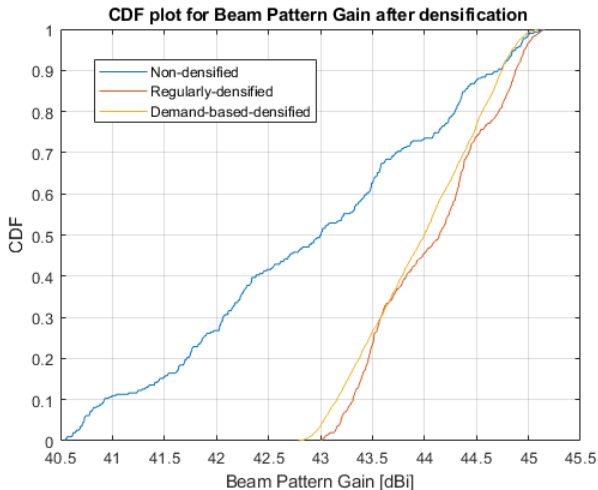| Satellite longitude	13 degree East (GEO)
Beam radiation pattern	Provided by ESA in CGD [64] project
User link bandwidth, B	500 MHz
Roll-off factor	20%
Terminal antenna diameter	0.6 m
Terminal antenna efficiency	60%
DL wavelength	0.01538 m

Fig. 15: Beam Pattern gain after densification

A. Beam pattern analysis

The beam pattern for 4 non-densified beams along with 10 neighbouring beams are shown in Figure 12. Furthermore, the gain values in dBi are shown using the color bar in Figure 14 for all the beam pattern plots. Evidently, there are more regions with lower values of beam pattern gain (near the beam borders). Any possible high demand users in this region are expected to experience poor SINR. Similarly, beam pattern for 16 regularly-densified beams and 13 demand driven densified beams along with the neighbouring beams are shown in Figure 13 and Figure 14 respectively. Evidently, in both the densified beam patterns, most of the regions show higher values of beam pattern gain. Hence, densification improves the beam pattern gain values.

Furthermore, Figure 15 provides the CDF plot of the beam pattern gain. Evidently, the beam pattern gain values have improved considerably (worst case gain of approximately 2.5 dB) after densification. Furthermore, regularly densified beam pattern shows slightly better performance against the demand based densification.

B. Impact of densification with 4 color frequency reuse

The table II provides the bandwidth and power allocation for 4CR frequency analysis. For fair comparison, we consider equal power and bandwidth distribution before and after densification. At target hot-spot area, the satellite total radiated power is considered as 166.67 W. This power is shared between 4 beams in the case of non-densified scenario and furthermore, it is shared between 16 beams in the regularly

densified case and between 13 beams in the case of demand-driven densified case. Also, for 4CR frequency reuse, the total bandwidth of 500 MHz is divided into two, considering that the additional two colors could be obtained from polarization.

TABLE II: Power and Bandwidth allocation for 4CR frequency reuse

Beam Pattern	Power per beam	Bandwidth per beam
Non-densified beam	41.67 W	250 MHz
Regularly densified beam	10.4175 W	250 MHz
Demand-driven densified beam	12.8215 W	250 MHz

The Figure 16 shows the CDF plots of the per-beam average SINR and Figure 17 shows the Average user SINR for 4CR frequency reuse. The SINR performance degrades from non-densified case to demand-driven densified case and further decreases when the densification is carried with 16 regular beams. Evidently, SINR decrease with the increase in the number of beams. This is majorly because higher number of beams will increase the interference signal.

Figure 18 shows the per beam average capacity and Figure 19 shows the mean capacity for 4CR frequency reuse. As the bandwidth per beam do not change upon densification with 4CR frequency reuse, the DVB-S2X defined capacity results are inline with the previously discussed SINR performance.

Due to reduced SINR with the increase in the number of beams, the densification perform poorly in terms of offered per beam average capacity by using same 4CR frequency reuse. Hence, in the following sections, we evaluate the performance of densification with other frequency reuse factors. However, from the Figure 20, the system capacity has increased considerably after densification, especially for demand driven densification.

Furthermore, we defined demand of beam k as $D_k = \sum_{n \in k} d_n$, where d_n is the demand of a user n served by beam k. The offered capacity per beam is denoted by $C_k = \sum_{n \in k} c_n$, where c_n is the offered capacity to a user n served by beam k. Then, we define mean demand satisfaction of beam k in percentage as $DS_k = \frac{C_k}{D_k} \times 100$, such that if $DS_k > 100$, then $DS_k = 100, \forall k$. Furthermore, we define the system demand satisfaction as $DS_{sys} = \sum_{k=1}^{K} DS_k$. Figure 21 shows the demand satisfaction before and after densification while using 4CR frequency reuse scheme. Evidently, it can seen that the mean beam demand satisfaction has increased upon regular densification and further increased by demand driven densification.

C. Impact of densification with full frequency reuse and precoding

In this section, we evaluate the benefits of precoding (Minimum Mean Square Error (MMSE) precoder [56]) with beam densification. The major advantage of precoding is that the total available system bandwidth (500 MHz) is now available for all beams. Furthermore, as we had exploited the benefits of polarisation in other cases, for fair comparison, the available bandwidth per beam while using FFR is 1000 MHz. The power allocation remains same as described in Table II.
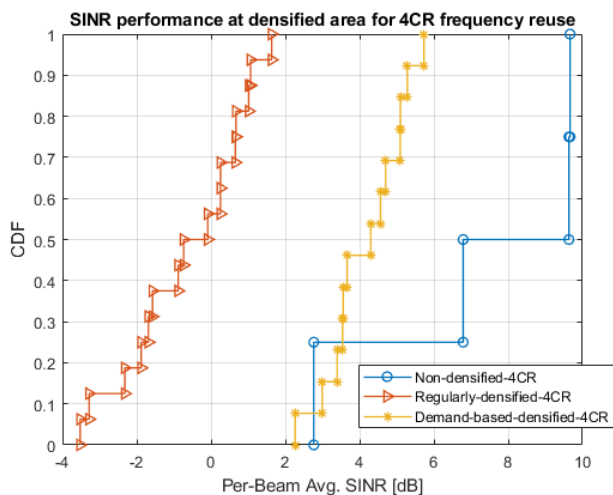
Fig. 16: SINR performance at densified area for 4CR frequency reuse
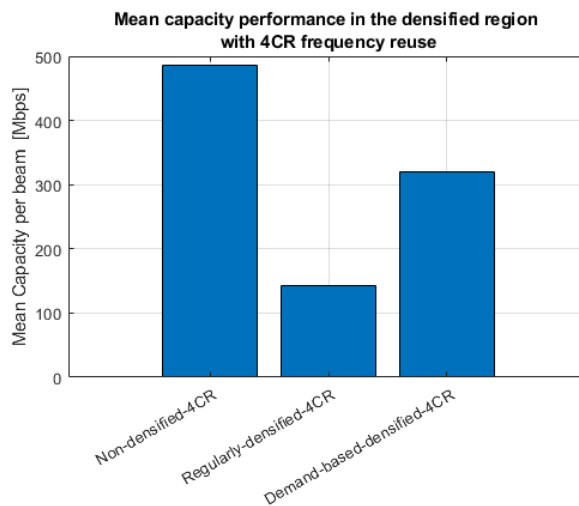

Fig. 17: SINR performance at densified area for 4CR frequency reuse

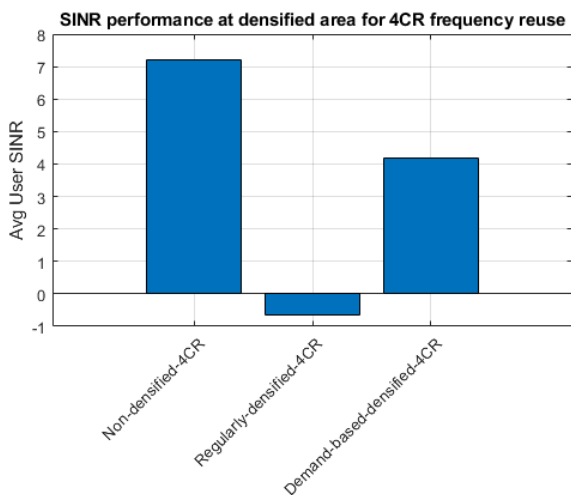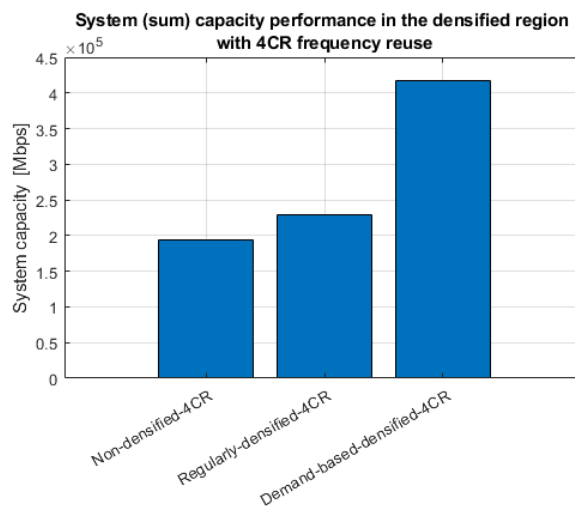Fig. 18: Capacity performance based on DVB-S2X at densified area for 4CR frequency reuse

Fig. 19: Mean capacity performance based on DVB-S2X at densified area for 4CR frequency reuse

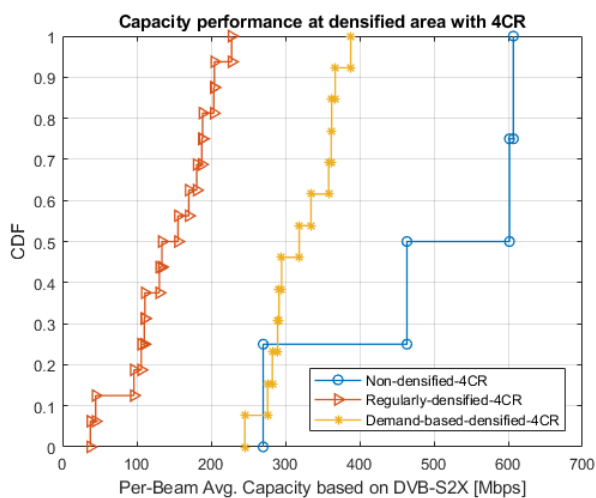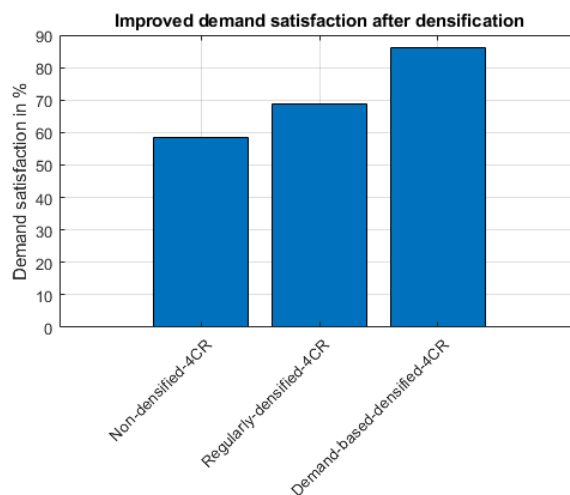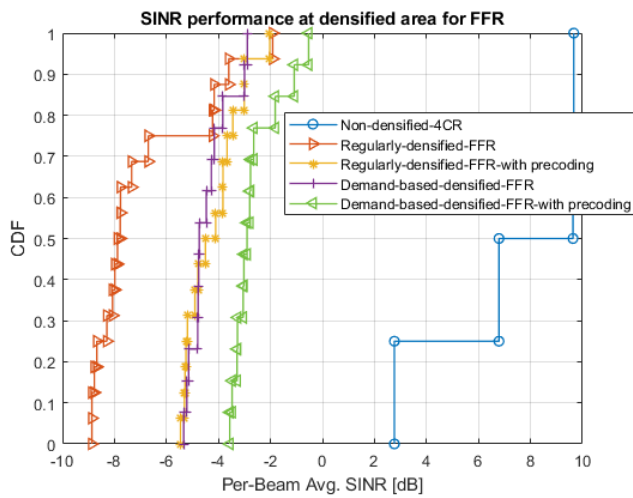Fig. 20: System (sum) capacity performance based on DVB-S2X at densified area for 4CR frequency reuse

Fig. 21: Demand satisfaction with 4CR frequency reuse

Fig. 22: SINR performance of Precoding with FFR
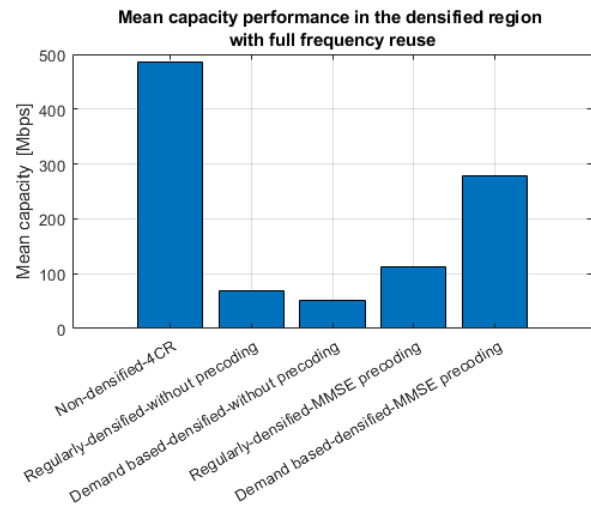
Fig. 25: Mean capacity performance based on DVB-S2X at densified area for full frequency reuse
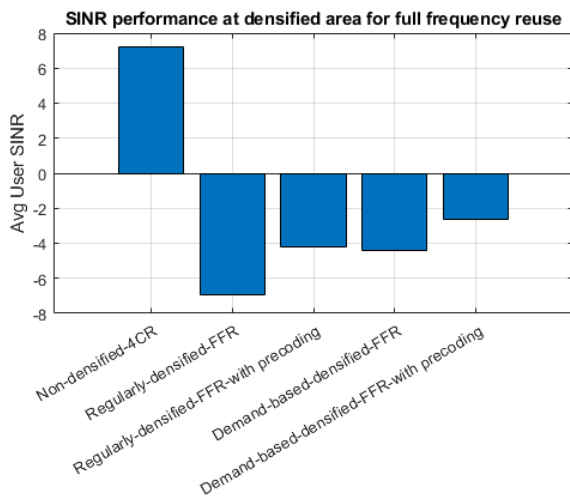

Fig. 23: SINR performance at densified area for full frequency reuse
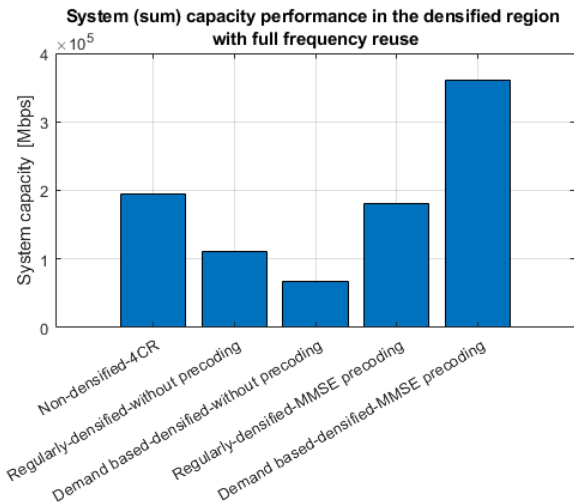

Fig. 26: System (sum) capacity performance based on DVB-S2X at densified area for full frequency reuse
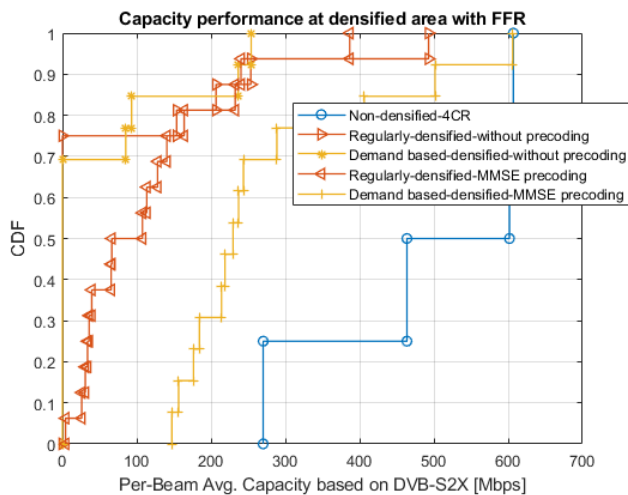

Fig. 24: Capacity performance based on DVB-S2X at densified area for full frequency reuse
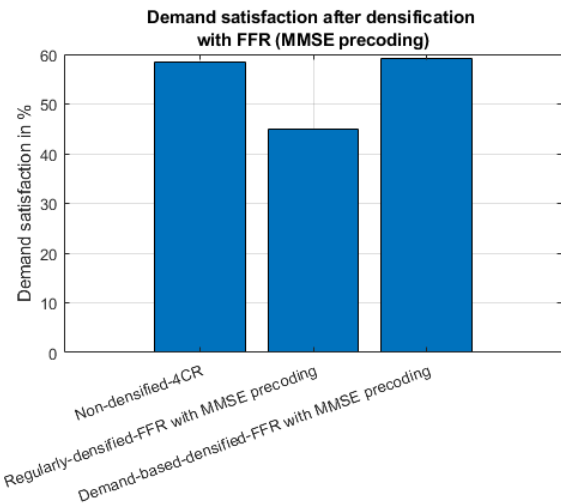

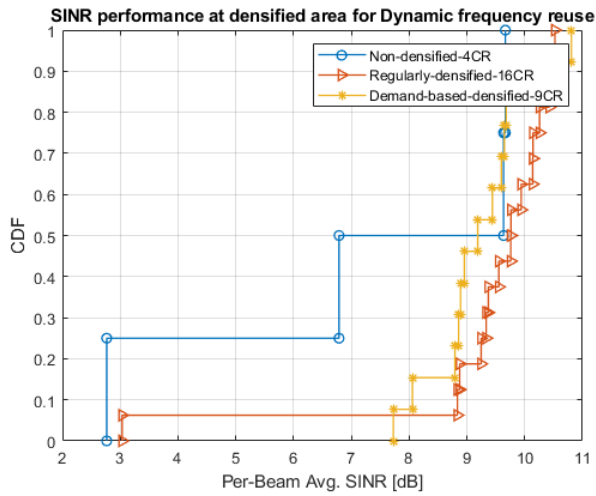Fig. 27: Demand satisfaction with full frequency reuse

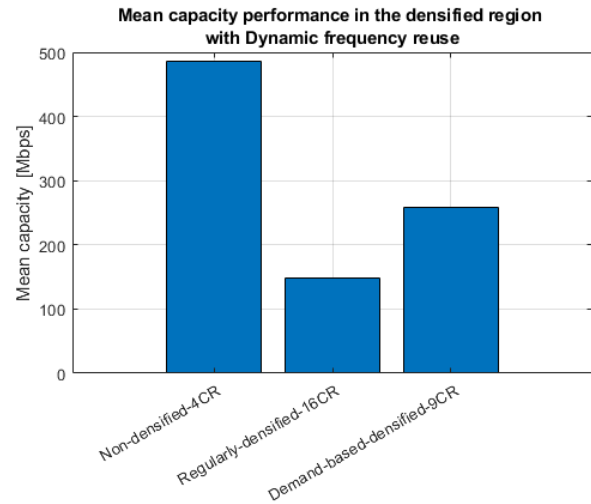Fig. 28: SINR performance at densified area for DFR frequency reuse

Fig. 29: SINR performance at densified area for DFR frequency reuse

Fig. 30: Capacity performance based on DVB-S2X at densified area for Dynamic frequency reuse

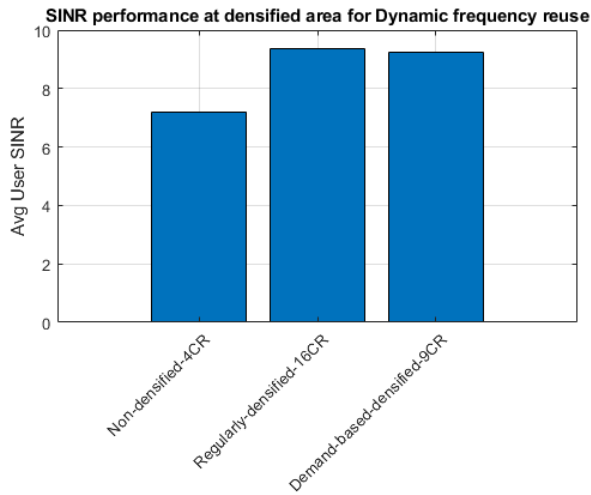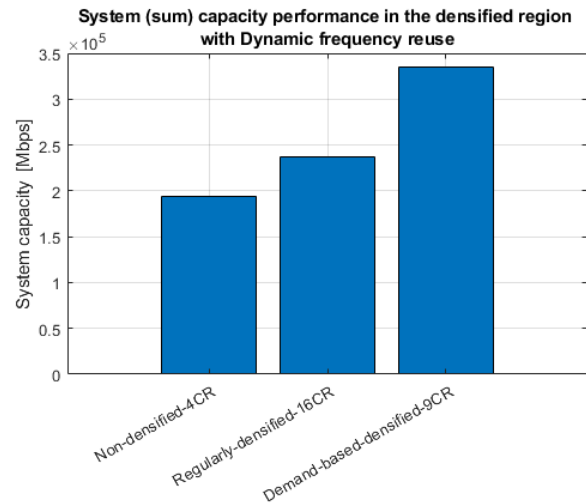Fig. 31: Mean capacity performance based on DVB-S2X at densified area for dynamic frequency reuse
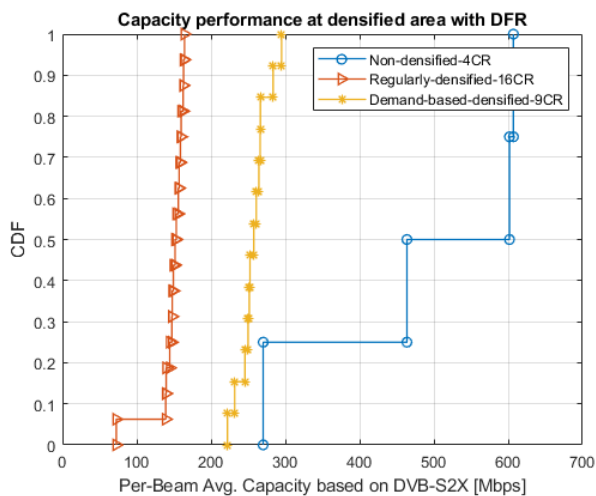

Fig. 32: System (sum) capacity performance based on DVB-S2X at densified area for dynamic frequency reuse
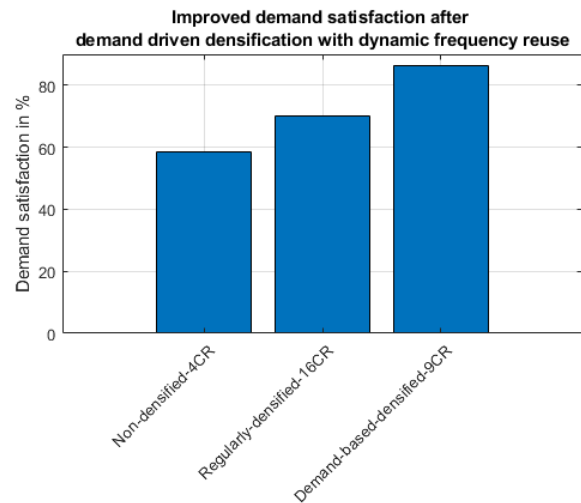

Fig. 33: Demand satisfaction with dynamic frequency reuse

The Figure 22 shows the CDF plots of the per-beam average SINR and Figure 23 shows the Average user SINR for full frequency reuse. Both regular and demand based densification using FFR without precoding perform very poor. Furthermore, demand driven densification using FFR with precoding has performed slightly better than regular densification using FFR with precoding. Conclusively, it can be inferred that using full frequency reuse schemes, the SINR can degrade considerably after densification. Such poor performance in SINR is due to strong levels of interference created by increased number of beams after densification.

Figure 24 shows the per beam average capacity and Figure 25 shows the mean capacity for full frequency reuse. When precoding is not considered, in both regular and demand driven densification, we notice that the performance is very poor due to poor SINR performance and the system fails to satisfy the minimum link budget requirements. On the other hand, when precoding is considered with densification, the DVB-S2X defined capacity is relatively good even with poor SINR performance, as the bandwidth per beam availability is very high for FFR. Furthermore, from Figure 26, system capacity increases after densification, especially for demand based densification.

Figure 27 shows the demand satisfaction before and after densification while using FFR scheme. We consider only the results with precoding as the system performs poor without precoding. Evidently, it can seen that the mean beam demand satisfaction does not gain much with densification.

D. Impact of densification with Dynamic frequency reuse

In this section we evaluate the performance of other dynamic color frequency reuse schemes. For regular beam densification we use 16CR color frequency reuse scheme as we expect its interference levels to be similar to 4CR non densified beams. Furthermore, for demand driven beam densification, we use optimized color coding proposed in section V. The power allocation and bandwidth available for dynamic frequency reuse is shown in the table III.

The Figure 28 shows the CDF plots of the per-beam average SINR and Figure 29 shows the Average user SINR for dynamic frequency reuse. Regular densification with 16 CR has resulted to gain high in SINR. Furthermore, demand driven densification with dynamic color coding (9CR frequency reuse) has performed slightly poor than demand driven densification with 16CR frequency reuse. However, the worst case SINR of demand driven densification is better in comparison to Regular densification with 16 CR frequency reuse. Conclusively, it can be inferred that using higher order frequency reuse schemes, the SINR can improve considerably after densification.

Figure 30 shows the per beam average capacity and Figure 31 shows the mean capacity for dynamic frequency reuse. With the increase in colors, the available bandwidth decreases and hence DVB-S2X defined capacity reduces for 9CR frequency reuse and further reduces for 16CR frequency reuse. However, from the Figure 32, the system capacity is still better after densification, especially for demand based densification with 9CR frequency reuse.

TABLE III: Power and Bandwidth allocation for dynamic frequency reuse

Beam Pattern	Power per beam	Bandwidth per beam
Non-densified beam	41.67 W	250 MHz
Regularly densified beam	10.4175 W	62.5 MHz
Demand-driven densified beam	12.8215 W	111.11 MHz

The demand satisfaction for dynamic frequency reuse is shown in Figure 33. Evidently, the demand satisfaction has increased considerably after densification, especially for demand driven densification with 9CR reuse.

E. Comparative Analysis of the proposed demand driven densification with the benchmark: demand driven Voronoi partitioning algorithm [65]

As part of our effort to enhance the authenticity and relevance of our proposed scheme, we also compared it to a benchmark scheme defined in [65], which provides multi-beam coverage of a Region of Interest (ROI) in a multi-beam satellite communication system. This benchmark is also designed to account for non-uniform traffic demand density over the ROI and serves as an adequate benchmark to compare our proposed scheme.

The benchmark [65] did not optimize the number of beams. Hence, we tested the approach proposed in [65] for the beam design assuming that the number of beams are four, which is in-line with the number of beams of the conventional beam pattern at the ROI. Accordingly, we partitioned the Region of Interest (ROI) into four non-overlapping cells (V1-V4) using the Voronoi diagram in such a way that the traffic demand associated with the cells is substantially uniform. As stated in [65], we iterative adjusted the positions of the center of the Voronoi cell and evaluated the uniformity of distribution and is shown in the Figure 34. In the following step, we generated four satellite beams to cover specific cells, and computed the capacity offered using a methodology similar to that used in the preceding sections. To minimize interference levels between beams that share the same frequency band and polarization state, we adopted the frequency band/polarization state pair allocation approach recommended in [65].

The results depicted in Figure 35 indicate that the per-beam average capacity of the proposed scheme is lower than that of the benchmark. This is not unexpected, given that the benchmark benefits from greater bandwidth availability owing to lower frequency and polarization reuse. However, as shown in Figure 36, our proposed scheme achieves a higher sum capacity due to densification.

Importantly, Figure 37 reveals that our proposed scheme outperforms the benchmark in terms of demand satisfaction. Notably, the benchmark achieves better demand satisfaction than the fixed beam design of the non-densified-4CR case (discussed in the previous sections and has demand satisfaction of 59%) by more evenly distributing the total demand across all the beams. In conclusion, our proposed scheme leverages densification to achieve a higher sum capacity, while still providing excellent demand satisfaction.
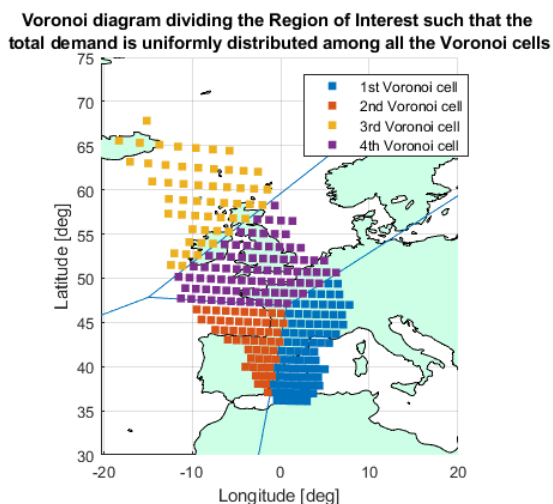
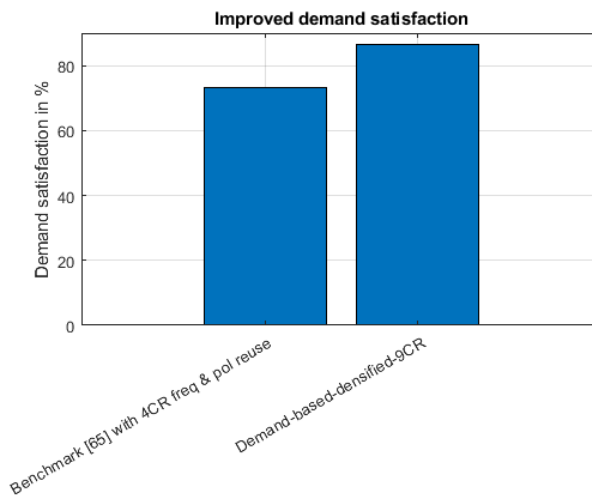Fig. 34: Region of Interest (ROI) divided using Voronoi partitioning algorithm

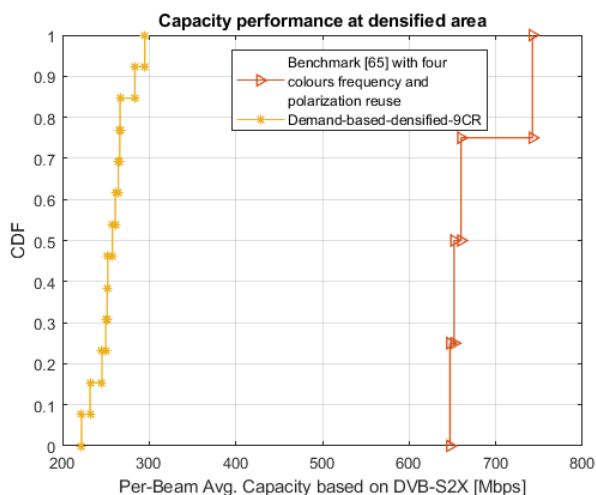
Fig. 35: Capacity performance comparison at the ROI

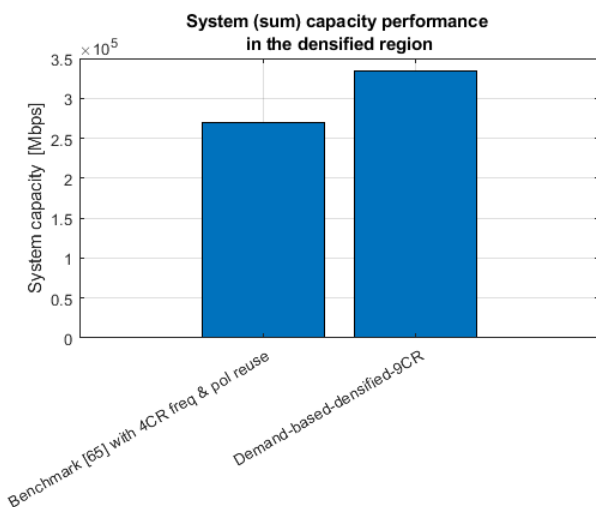Fig. 36: Improved sum capacity at the ROI

Fig. 37: Improved demand satisfaction at the ROI
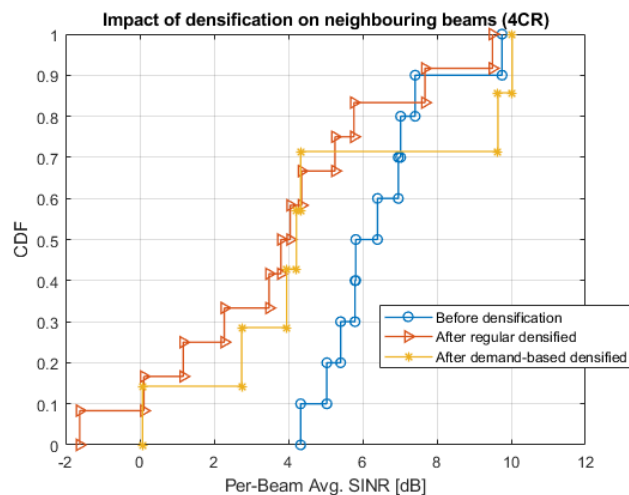
Fig. 38: CDF plots of per beam avg SNIR on neighbouring beams

F. Performance evaluation neighbouring beams of densification

In this section, we assess the impact of densification on the neighbouring beams of the densified region. Again, we consider unicast scheduling with $K = 10$ users scheduled in $K = 10$ neighbouring beams where each of the user position in the neighbouring beams are randomly selected.

Figure 38 and Figure 39 show the impact of densification on the neighbouring beams of the densified region. From CDF plot of Figure 38, we can infer that values of per beam average SINR of the neighbouring beams reduce considerably due to regular densification. However, after the proposed demand based densification, even though per beam average SINR of the neighbouring beams is still lower than the non densified case, it has relatively improved in comparison to regular densification. Furthermore from Figure 39, the average user SINR of the neighbouring beams drops after regular densification. However, it improves considerably when we consider the proposed demand based densification. This is majorly

Fig. 39: Average user SINR on neighbouring beams

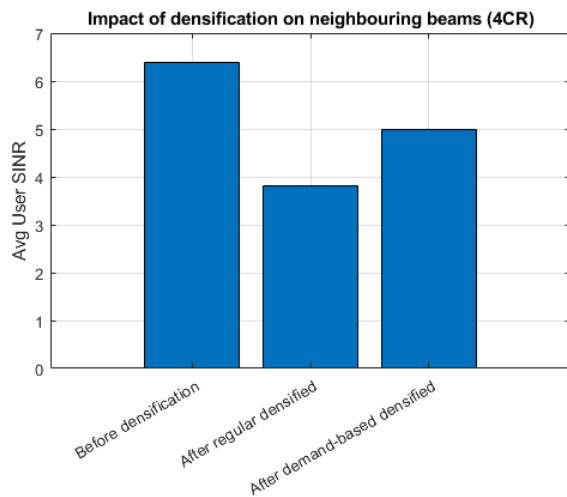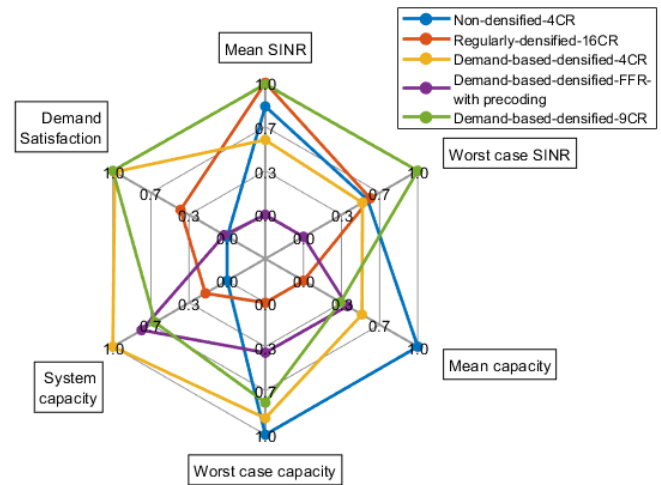

Fig. 40: Radar chart summarising the results

because, regular densification increases the beam overlap on the neighbouring beams. However, when we consider the demand based densification, such overlap on the neighbouring beams is considerably reduced.

Also, due to densification, even though the performance of the neighbouring beams are slightly degraded with increased interference levels, performance loss is acceptable as the demand in the neighbouring beams are relatively low. Such impact in the neighboring beams in fact reduces the gap between the demand and the offered capacity, which is eventually better resource management.

VII. CONCLUSION

In this work, we first discuss the conventional multi-beam GEO satellite system and its failure to provide demand satisfaction in high demand hot spot regions. Accordingly, we then propose a regular beam densification as the first step in achieving demand satisfaction. Furthermore, considering the uneven demand distribution in the high demand region, we propose a novel dynamic beam densification procedure which leverages to choose ideal number of beams and their positions. Lastly, using graph theory, we propose a dynamic frequency allocation strategy to reduce the increased inter-beam interference upon beam densification.

Furthermore, the proposed solution is computationally expensive for an instantaneous adaptation. However, GEO satellite systems do not intend to adapt the beam planning in a matter of seconds or minutes. Beam densification is something that can be done eventually (e.g. twice a day) to match specific demand patterns that are easy to predict. In this sense, the requirements in terms of speed of computation are not that critical, as one can precalculate it well in advance. On the other hand, the impact in terms of signalling and user disconnection due to the beam planning change are minimize to very few events.

To summarize the result of this work, we use a two-dimensional radar chart in Figure 40, displaying multivariate data in the form of a chart of six quantitative variables (normalized) such as mean SINR, worst case SINR, mean capacity,

worst case capacity, system capacity and demand satisfaction. Evidently, the non-densified 4CR frequency reuse scheme fail to provide demand satisfaction with the least demand satisfaction score. Regularly densified 16CR frequency reuse scheme, slightly increases the demand satisfaction with good SINR performance but provides poor capacity results due to scarcity of the bandwidth. Furthermore, demand based densified 4CR frequency reuse provides good demand satisfaction and capacity performance but performs poor at the user SINR level. Notwithstanding, when same demand based scheme is considered with precoding, the user SINR levels are very poor. Furthermore, when the proposed demand based densified 9CR (dynamic frequency) is considered, it maximizes most of the metrics of the radar chart. Lastly, when we studied the impact of densification on the neighbouring beams, it was evident that after regular densification, the SINR performance of the neighbouring beams is affected. However, when we employ the proposed demand based densification, such adverse effects are considerably reduced. Conclusively, the proposed demand-based densification with dynamic frequency reuse is the best choice regarding most of the quantitative variables.

VIII. ACKNOWLEDGEMENT

REFERENCES

[1] L. Cottatellucci, M. Debbah, G. Gallinaro, R. Mueller, M. Neri, and R. Rinaldo, *Interference Mitigation Techniques for Broadband Satellite Systems*. [Online]. Available: https://arc.aiaa.org/doi/abs/10.2514/6.2006-5348
[2] Y. Couble, C. Rosenberg, E. Chaput, J.-B. Dupé, C. Baudoin, and A.-L. Beylot, "Two-color scheme for a multi-beam satellite return link: Impact of interference coordination," *IEEE Journal on Selected Areas in Communications*, vol. 36, no. 5, pp. 993–1003, 2018.
[3] O. Kilic and A. I. Zaghloul, "Interference in cellular satellite systems," in *Satellite Communications*, N. Diodato, Ed. Rijeka: IntechOpen, 2010, ch. 15. [Online]. Available: https://doi.org/10.5772/9997
[4] A. Mehrotra, "Cellular radio performance engineering," Boston, 1994.

[5] E. Lier and D. Purdy, "Techniques to maximize communication traffic capacity in multi-beam satellite active phased array antennas for non-uniform traffic model," in *Proceedings 2000 IEEE International Conference on Phased Array Systems and Technology (Cat. No.00TH8510)*, 2000, pp. 505–508.

[6] "Satellite traffic emulator," *SnT, University of Luxembourg*, 2021. [Online]. Available: https://wwwfr.uni.lu/snt/research/sigcom/sw_simulators/satellite_traffic_emulator

[7] O. Kodheli, E. Lagunas, N. Maturo, S. K. Sharma, B. Shankar, J. F. M. Montoya, J. C. M. Duncan, D. Spano, S. Chatzinotas, S. Kisseleff, J. Querol, L. Lei, T. X. Vu, and G. Goussetis, "Satellite communications in the new space era: A survey and future challenges," *IEEE Communications Surveys Tutorials*, vol. 23, no. 1, pp. 70–109, 2021.

[8] R. De Gaudenzi, M. Luise, and L. Sanguinetti, "The open challenge of integrating satellites into (beyond-) 5g cellular networks," *IEEE Network*, vol. 36, no. 2, pp. 168–174, 2022.

[9] F. Vidal, H. Legay, G. Goussetis, M. Vigueras, S. Tubau, and J. Gayrard, "A methodology to benchmark flexible payload architectures in a mega-constellation use case," *International Journal of Satellite Communications and Networking*, vol. 39, 03 2020.

[10] L. Chen, E. Lagunas, S. Chatzinotas, and B. Ottersten, "Satellite broadband capacity-on-demand: Dynamic beam illumination with selective precoding," in *2021 29th European Signal Processing Conference (EUSIPCO)*, 2021, pp. 900–904.

[11] Z. Lin, Z. Ni, L. Kuang, C. Jiang, and Z. Huang, "Dynamic beam pattern and bandwidth allocation based on multi-agent deep reinforcement learning for beam hopping satellite systems," *IEEE Transactions on Vehicular Technology*, vol. 71, no. 4, pp. 3917–3930, 2022.

[12] F. G. Ortiz-Gomez, L. Lei, E. Lagunas, R. Martinez, D. Tarchi, J. Querol, M. A. Salas-Natera, and S. Chatzinotas, "Machine learning for radio resource management in multibeam geo satellite systems," *Electronics*, vol. 11, no. 7, 2022. [Online]. Available: https://www.mdpi.com/2079-9292/11/7/992

[13] T. S. Abdu, S. Kisseleff, E. Lagunas, and S. Chatzinotas, "Flexible resource optimization for geo multibeam satellite communication system," *IEEE Transactions on Wireless Communications*, vol. 20, no. 12, pp. 7888–7902, 2021.

[14] G. Cocco, T. de Cola, M. Angelone, Z. Katona, and S. Erl, "Radio Resource Management Optimization of Flexible Satellite Payloads for DVB-S2 Systems," *IEEE Transactions on Broadcasting*, vol. 64, no. 2, pp. 266–280, Jun. 2018.

[15] A. Freedman, D. Rainish, and Y. Gat, "Beam Hopping – How To Make it Possible," in *Proc. of Ka and Broadband Communication Conference*, Oct. 2015.

[16] P. Angeletti, D. F. Prim, and R. Rinaldo, "Beam hopping in multi-beam broadband satellite systems: System performance and payload architecture analysis," in *24th AIAA International Communications Satellite Systems Conference*. [Online]. Available: https://arc.aiaa.org/doi/abs/10.2514/6.2006-5376

[17] C. N. Efrem and A. D. Panagopoulos, "Dynamic Energy-Efficient Power Allocation in Multibeam Satellite Systems," *IEEE Wireless Communications Letters*, vol. 9, no. 2, pp. 228–231, 2020.

[18] A. I. Aravanis, B. Shankar M. R., P. Arapoglou, G. Danoy, P. G. Cottis, and B. Ottersten, "Power Allocation in Multibeam Satellite Systems: A Two-Stage Multi-Objective Optimization," *IEEE Transactions on Wireless Communications*, vol. 14, no. 6, pp. 3171–3182, June 2015.

[19] P. Angeletti and J. Lizarraga Cubillos, "Traffic balancing multibeam antennas for communication satellites," *IEEE Transactions on Antennas and Propagation*, vol. 69, no. 12, pp. 8291–8303, 2021.

[20] R. De Gaudenzi, P. Angeletti, D. Petrolati, and E. Re, "Future technologies for very high throughput satellite systems," *International Journal of Satellite Communications and Networking*, vol. 38, no. 2, pp. 141–161, 2020. [Online]. Available: https://onlinelibrary.wiley.com/doi/abs/10.1002/sat.1327

[21] G. Toso, P. Angeletti, and C. Mangenot, "Multibeam antennas based on phased arrays: An overview on recent esa developments," in *The 8th European Conference on Antennas and Propagation (EuCAP 2014)*, 2014, pp. 178–181.

[22] "The state of broadband - international telecommunication union (itu): People-centred approaches for universal broadband," Sep 2021. [Online]. Available: https://www.itu.int/dms_pub/itu-s/opb/pol/S-POL-BROADBAND.19-2018-PDF-E.pdf

[23] "Ads-b exchange - world's largest co-op of unfiltered flight data," 2021. [Online]. Available: https://www.adsbexchange.com/data/

[24] "Ais ship tracking of marine traffic," 2021. [Online]. Available: https://www.vesselfinder.com/.

[25] NASA, "Nasa, socioeconomic data and applications center (sedac)," 2021. [Online]. Available: http://sedac.ciesin.columbia.edu.

[26] H. Al-Hraishawi, E. Lagunas, and S. Chatzinotas, "Traffic simulator for multibeam satellite communication systems," in *2020 10th Advanced Satellite Multimedia Systems Conference and the 16th Signal Processing for Space Communications Workshop (ASMS/SPSC)*, 2020, pp. 1–8.

[27] "Revolve: Radio technologies for broadband connectivity in a rapidly evolving space ecosystem: Innovating agility, throughput, power, size and cost." [Online]. Available: https://ec.europa.eu/research/participants/documents/download Public?documentIds=080166e5b87884eaamp;appId=PPGMS

[28] M. Schneider, C. Hartwanger, and H. Wolf, "Antennas for Multiple Spot Beam Satellites," *CEAS Space Journal*, vol. 2, pp. 59–66, Aug. 2011.

[29] C. Leclerc, M. Romier, A. Annabi, and H. Aubert, "Ka-band multiple feed per beam antenna architecture based on interleaved 3-d directional couplers," in *2013 IEEE-APS Topical Conference on Antennas and Propagation in Wireless Communications (APWC)*, 2013, pp. 367–369.

[30] P. Bosshard *et al.*, "Space HTS/V-HTS Multiple Beam Antennas subsystems on the right track," *Proc. European Conference on Antennas and Propag. (EuCAP), Davos, Switzerland*, vol. 2, pp. 1–5, 2016.

[31] W. M. Abdel-Wahab, H. Al-Saedi, M. Raeis-Zadeh, E. H. Mirza Alian, A. Ehsandar, G. Chen, A. Palizban, N. Ghafarian, H. El-Sawaf, M. R. Nezhad-Ahmadi, and S. Safavi Naeini, "Affordable large scale active-phased array antenna for ka-band mobile satcom applications," in *2019 13th European Conference on Antennas and Propagation (EuCAP)*, 2019, pp. 1–4.

[32] M. Cooley, "Phased Array-Fed Reflector (PAFR) Antenna Architectures for Space-Based Sensors ," *IEEE Aerospace Conference*, pp. 1–11, 2015.

[33] W. Li, X. Huang, and H. Leung, "Performance evaluation of digital beamforming strategies for satellite communications," *IEEE Transactions on Aerospace and Electronic systems*, vol. 40, no. 1, pp. 12–26, 2004.

[34] P. Angeletti, G. Gallinaro, M. Lisi, and A. Vernucci, "On-ground digital beamforming techniques for satellite smart antennas," *Proc. 19th AIAA, Toulouse, France*, pp. 1–8, 2001.

[35] M. Barrett and F. Coromina, "Development and implementation of an adaptive digital beamforming network for satellite communication systems," in *1991 Sixth International Conference on Digital Processing of Signals in Communications*. IET, 1991, pp. 10–15.

[36] D. Sikri and R. M. Jayasuriya, "Multi-beam phased array with full digital beamforming for satcom and 5g," *5G Phased Array Technologies*, p. 30, 2019.

[37] C. Forrester, "Ses adopts digital satellite payloads," Jun 2016. [Online]. Available: https://advanced-television.com/2016/06/29/ses-adopts-digital-satellite-payloads/

[38] N. Mazzali, M. R. Bhavani Shankar, and B. Ottersten, "On-board signal predistortion for digital transparent satellites," in *2015 IEEE 16th International Workshop on Signal Processing Advances in Wireless Communications (SPAWC)*, 2015, pp. 535–539.

[39] U. du Luxembourg, "Prosat: On-board processing techniques for high throughput satellites." [Online]. Available: https://wwwfr.uni.lu/snt/research/sigcom/projects/prosat_on_board _processing_techniques_for_high_throughput_satellites

[40] V. Sulli, F. Santucci, M. Faccio, and D. Giancristofaro, "Performance of satellite digital transparent processors through equivalent noise," *IEEE Transactions on Aerospace and Electronic Systems*, vol. 54, no. 6, pp. 2643–2661, 2018.

[41] J. Liu, M. Sheng, L. Liu, and J. Li, "Network densification in 5g: From the short-range communications perspective," *IEEE Communications Magazine*, vol. 55, no. 12, pp. 96–102, 2017.

[42] D. López-Pérez, M. Ding, H. Claussen, and A. H. Jafari, "Towards 1 Gbps/UE in Cellular Systems: Understanding Ultra-Dense Small Cell Deployments," *IEEE Communications Surveys Tutorials*, vol. 17, no. 4, pp. 2078–2101, 2015.

[43] J. Hoadley and P. Maveddat, "Enabling small cell deployment with hetnet," *IEEE Wireless Communications*, vol. 19, no. 2, pp. 4–5, 2012.

[44] N. Bhushan, J. Li, D. Malladi, R. Gilmore, D. Brenner, A. Damnjanovic, R. T. Sukhavasi, C. Patel, and S. Geirhofer, "Network densification: the dominant theme for wireless evolution into 5g," *IEEE Communications Magazine*, vol. 52, no. 2, pp. 82–89, 2014.

[45] S. Seewald and D. Manteuffel, "Design approach for modular millimeter wave beamforming antenna arrays for 5g pico-cells," in *2019 IEEE-APS Topical Conference on Antennas and Propagation in Wireless Communications (APWC)*, 2019, pp. 174–177.

[46] W.-S. Chen and H.-J. Lin, "Dual-polarization slot antenna array with resonant cavities for small-cell base station applications," in *2015 IEEE*

This article has been accepted for publication in IEEE Transactions on Aerospace and Electronic Systems. This is the author's version which has not been fully edited and content may change prior to final publication. Citation information: DOI 10.1109/TAES.2023.3278253

20

4th Asia-Pacific Conference on Antennas and Propagation (APCAP), 2015, pp. 58–59.

[47] Z. N. Chen, X. Qing, X. Tang, W. E. Liu, and R. Xu, "Phased array metantennas for satellite communications," *IEEE Communications Magazine*, vol. 60, no. 1, pp. 46–50, 2022.

[48] P. J. Honnaiah, N. Maturo, S. Chatzinotas, S. Kisseleff, and J. Krause, "Demand-based adaptive multi-beam pattern and footprint planning for high throughput GEO satellite systems," *IEEE Open Journal of the Communications Society*, vol. 2, pp. 1526–1540, 2021.

[49] H. Chaker, N. Maturo, S. Chatzinotas, H. Chougrani, W. A. Martins, and J. Grotz, "Enablers for matching demand in geo multi-beam satellites: dynamic beamforming, precoding, or both?" in *38th International Communications Satellite Systems Conference (ICSSC 2021)*, vol. 2021, 2021, pp. 104–111.

[50] F. G. Ortiz-Gomez, L. Lei, E. Lagunas, R. Martinez, D. Tarchi, J. Querol, M. A. Salas-Natera, and S. Chatzinotas, "Machine learning for radio resource management in multibeam geo satellite systems," *Electronics*, vol. 11, no. 7, 2022. [Online]. Available: https://www.mdpi.com/2079-9292/11/7/992

[51] A. Guidotti and A. Vanelli-Coralli, "Design trade-off analysis of precoding multi-beam satellite communication systems," in *2021 IEEE Aerospace Conference (50100)*, 2021, pp. 1–12.

[52] M. Á. Vázquez, A. Perez-Neira, D. Christopoulos, S. Chatzinotas, B. Ottersten, P.-D. Arapoglou, A. Ginesi, and G. Taricco, "Precoding in multibeam satellite communications: Present and future challenges," *IEEE Wireless Communications*, vol. 23, no. 6, pp. 88–95, 2016.

[53] S. Kisseleff, E. Lagunas, J. Krivochiza, J. Querol, N. Maturo, L. Martinez Marrero, J. C. Merlano Duncan, and S. Chatzinotas, "Centralized gateway concept for precoded multi-beam GEO satellite networks," in *VTC2021-Fall Workshop on Evolution of Non-Terrestrial Networks Toward 6G,*, 2021.

[54] ETSI, "Digital video broadcasting (dvb); second generation framing structure, channel coding and modulation systems for broadcasting, interactive services, news gathering and other broadband satellite applications; part 2: DVB-S2 extensions (DVB-S2X)," *Digital Video Broadcasting (DVB)*, vol. ETSI EN 302 307-2 V1.1.1, 2014-10. [Online]. Available: https://www.etsi.org/deliver/etsi_en/302300_302399/30230702/01.01.01_20/en_30230702v010101a.pdf

[55] A. I. Perez-Neira, M. A. Vazquez, M. B. Shankar, S. Maleki, and S. Chatzinotas, "Signal processing for high-throughput satellites: Challenges in new interference-limited scenarios," *IEEE Signal Processing Magazine*, vol. 36, no. 4, pp. 112–131, 2019.

[56] J. Krivochiza, J. C. M. Duncan, J. Querol, N. Maturo, L. M. Marrero, S. Andrenacci, J. Krause, and S. Chatzinotas, "End-to-end precoding validation over a live GEO satellite forward link," *IEEE Access*, pp. 1–1, 2021.

[57] T. Iguchi, D. G. Mixon, J. Peterson, and S. Villar, "On the tightness of an SDP relaxation of k-means," *CoRR*, vol. abs/1505.04778, 2015. [Online]. Available: http://arxiv.org/abs/1505.04778

[58] Q. Du, V. Faber, and M. Gunzburger, "Centroidal voronoi tessellations: Applications and algorithms," *SIAM Review*, vol. 41, no. 4, pp. 637–676, Jan. 1999. [Online]. Available: https://doi.org/10.1137/s0036144599352836

[59] P. J. Rousseeuw, "Silhouettes: A graphical aid to the interpretation and validation of cluster analysis," *Journal of Computational and Applied Mathematics*, vol. 20, pp. 53–65, Nov. 1987. [Online]. Available: https://doi.org/10.1016/0377-0427(87)90125-7

[60] R. Tibshirani, G. Walther, and T. Hastie, "Estimating the number of clusters in a data set via the gap statistic," *Journal of the Royal Statistical Society: Series B (Statistical Methodology)*, vol. 63, no. 2, pp. 411–423, 2001. [Online]. Available: https://doi.org/10.1111/1467-9868.00293

[61] D. L. Davies and D. W. Bouldin, "A cluster separation measure," *IEEE Transactions on Pattern Analysis and Machine Intelligence*, vol. PAMI-1, no. 2, pp. 224–227, 1979.

[62] S. Maher, M. Miltenberger, J. P. Pedroso, D. Rehfeldt, R. Schwarz, and F. Serrano, "PySCIPOpt: Mathematical programming in python with the SCIP optimization suite," in *Mathematical Software – ICMS 2016*. Springer International Publishing, 2016, pp. 301–307.

[63] K. Bestuzheva, M. Besançon, W.-K. Chen, A. Chmiela, T. Donkiewicz, J. van Doornmalen, L. Eifler, O. Gaul, G. Gamrath, A. Gleixner, L. Gottwald, C. Graczyk, K. Halbig, A. Hoen, C. Hojny, R. van der Hulst, T. Koch, M. Lübbecke, S. J. Maher, F. Matter, E. Mühmer, B. Müller, M. E. Pfetsch, D. Rehfeldt, S. Schlein, F. Schlösser, F. Serrano, Y. Shinano, B. Sofranac, M. Turner, S. Vigerske, F. Wegscheider, P. Wellner, D. Weninger, and J. Witzig, "The SCIP Optimization Suite 8.0," Optimization Online, Technical Report, December 2021. [Online]. Available: http://www.optimization-online.org/DB_HTML/2021/12/8728.html

[64] "Esa cgd - prototype of a centralized broadband gateway for precoded multi-beam networks," *SnT, University of Luxembourg*, 2021. [Online]. Available: https://wwwfr.uni.lu/snt/research/sigcom/projects/esa_cgd

[65] P. Angeletti and J. Camilo Lizarraga Cubillos, "Method and a system of providing multi-beam coverage of a region of interest in multi-beam satellite communication," *United States patents US9654201B2*, May 2017. [Online]. Available: https://patents.google.com/patent/US9654201

Puneeth Jubba Honnaiah has received his PhD in demand driven satellite resource optimization from Signal Processing and Satellite Communications group, SIGCOM, SnT, University of Luxembourg. He received the Bachelor of Engineering (BE) from Visvesvaraya Technological University (VTU), India in 2012 and the Master of Science (M.Sc.) from Hochschule Bremen- City University of Applied Sciences, Germany in 2017, all in Electronics and Communication engineering. Also, he has worked several years in the telecom industry and has expertise in satellite communication, GSM, LTE and 5G technologies.

Eva Lagunas Eva Lagunas received the MSc and PhD degrees in telecom engineering from the Polytechnic University of Catalonia (UPC), Barcelona, Spain, in 2010 and 2014, respectively. She was Research Assistant within the Department of Signal Theory and Communications, UPC, from 2009 to 2013. During the summer of 2009 she was a guest research assistant within the Department of Information Engineering, Pisa, Italy. From November 2011 to May 2012 she held a visiting research appointment at the Center for Advanced Communications (CAC), Villanova University, PA, USA. She joined the Interdisciplinary Centre for Security, Reliability and Trust (SnT), University of Luxembourg, first as a Research Associate, and in 2018 as Research Scientist. Her research interests include radio resource management and general wireless networks optimization.

Symeon Chatzinotas is currently Full Professor / Chief Scientist I and Co-Head of the SIGCOM Research Group at SnT, University of Luxembourg. In the past, he has been a Visiting Professor at the University of Parma, Italy and he was involved in numerous Research and Development projects for the National Center for Scientific Research Demokritos, the Center of Research and Technology Hellas and the Center of Communication Systems Research, University of Surrey. He received the M.Eng. degree in telecommunications from the Aristotle University of Thessaloniki, Thessaloniki, Greece, in 2003, and the M.Sc. and Ph.D. degrees in electronic engineering from the University of Surrey, Surrey, U.K., in 2006 and 2009, respectively. He was a co-recipient of the 2014 IEEE Distinguished Contributions to Satellite Communications Award, the CROWNCOM 2015 Best Paper Award and the 2018 EURASIC JWCN Best Paper Award. He has (co-)authored more than 400 technical papers in refereed international journals, conferences and scientific books. He is currently in the editorial board of the IEEE Open Journal of Vehicular Technology and the International Journal of Satellite Communications and Networking.

Jens Krause was born in Werdohl, Germany, in 1963. He received the Dipl.-Ing. degree in 1987 and the PhD degree in 1993, both in electrical engineering from University of Karlsruhe, Germany. He has held a scientific employee position at University of Karlsruhe from 1988 to 1993. From 1994 to 1996, he has been an RD engineer in the cable TV department of Richard Hirschmann GmbH in Germany. Since 1996, he works at the satellite operator SES S.A. in Luxembourg, with various positions in systems engineering. He represents SES in standardization organizations including ETSI and DVB. His research interests include satellite communications in general, modulation and coding, and signal processing for satellite communications.